minerals

MDPI

Article

Mesozoic Magmatic and Geodynamic Evolution in the Jiaodong Peninsula, China: Implications for the Gold and Polymetallic Mineralization

Bin Wang [1,2,3], Zhengjiang Ding [2,3,*], Zhongyi Bao [2,3,*], Mingchun Song [2,3], Jianbo Zhou [1], Junyang Lv [2,3], Shanshan Wang [2,3], Qibin Zhang [2,3] and Caijie Liu [2,3]

1 College of Earth Sciences, Jilin University, Changchun 130061, China
2 Shandong Provincial Engineering Laboratory of Application and Development of Big Data for Deep Gold Exploration, Weihai 264209, China
3 Shandong Provincial No. 6 Exploration Institute of Geology and Mineral Resources, Weihai 264209, China
* Correspondence: ytdzhj@126.com (Z.D.); sddzld2022@126.com (Z.B.)

Abstract: The intrusive age ranges of Linglong, Guojialing, Weideshan, and Laoshan granites in the Jiaodong Peninsula are 155–154 Ma, 131–130 Ma, 118–111 Ma, and 116 Ma, respectively. Together with the Shidao granite (227–200 Ma), five phases of magmatism can be classified by the time, all of which have different degrees of gold and polymetallic mineralization. The type of granites evolved from A–, S–type to I–, A–type from the Late Triassic to the Early Cretaceous, thus reflects the evolution of geodynamics in the Mesozoic, indicating the switch from North China Craton (NCC)–Yangtze Craton (YC) collision to subduction of the Paleo–Pacific Plate (PPP), with crustal thickening switching to lithospheric thinning and a compressional tectonic setting changing to an extensional setting. It directly leads to a series of extensional structures evolving in the Jiaodong Peninsula and demonstrates affinity for the extensive mineralization in the Early Cretaceous. The key markers of Jiaodong gold and polymetallic mineralization are magmatism, fluid activity and extensional structure. Extensive magmatic uplift and extensional structures in the Early Cretaceous formed the extensional tectonic system. During the formation process, a large proportion of crust and mantle materials exchanged and mixed, and the fluid interaction was highly active, resulting in a magmatic fluid metallogenic system, which provided favorable metallogenic conditions for gold and nonferrous metal hydrothermal deposits. Thus, a large-scale explosive mineralization occurred in Jiaodong in the middle and late Early Cretaceous.

Keywords: Mesozoic granite; geodynamic evolution; extensional structure; gold and polymetallic mineralization; Jiaodong Peninsula

Citation: Wang, B.; Ding, Z.; Bao, Z.; Song, M.; Zhou, J.; Lv, J.; Wang, S.; Zhang, Q.; Liu, C. Mesozoic Magmatic and Geodynamic Evolution in the Jiaodong Peninsula, China: Implications for the Gold and Polymetallic Mineralization. *Minerals* **2022**, *12*, 1073. https://doi.org/10.3390/min12091073

Academic Editor: Koen De Jong

Received: 12 July 2022
Accepted: 22 August 2022
Published: 25 August 2022

1. Introduction

Jiaodong Peninsula is located in the southeast margin of the North China Craton (NCC), and the junction of the Paleo–Tethys and the Paleo–Pacific metallogenic domains. The Mesozoic collision orogeny of the Yangtze Craton (YC) and the NCC superimposed the subduction–collision of the Paleo–Pacific Plate (PPP), resulting in intense crust–mantle interaction and frequent tectonic magmatism. The gold and polymetallic metallogenic conditions in this area are extremely superior. The deposits are mainly distributed in the Sanshandao and Zhaoyuan–Pingdu fault zones in the west, the Qixia fault zone in the middle, the Taocun–Zhuwu fault zone in the northeast margin of Jiaolai Basin, and the Jinniushan, Mizhan, and Lidao fault zones in the east. Dozens of super-large, large and medium-sized deposits have been discovered here, which is known as the "Jiaodong Metallogenic Province" in China [1]. Therefore, it is an interesting area for research related to deep continental subduction, destruction of the eastern NCC, and large-scale gold and polymetallic mineralization. The Jiaodong Peninsula has been an important gold producing

area since ancient times. The accumulated proven gold resources in the Jiaodong Peninsula have exceeded 5000 t, which has become the third largest gold metallogenic area in the world. Most of the deposits found in the western part of Jiaodong area are gold deposits, the central part is dominated by gold deposits with more associated metals, and the eastern part is dominated by polymetallic deposits [2,3]. Here is a natural laboratory for conducting research on the regularity of ore formation and providing demonstrations for prospecting.

The gold and polymetallic deposits are closely associated with Mesozoic granitic intrusions in Jiaodong Peninsula. Nevertheless, most previous studies focused on the Late Mesozoic gold mineralization, magmatism, and tectonism related to the Jurassic Linglong and Early Cretaceous Guojialing and Weideshan granites. Their genesis, tectonic setting, and evolution have been studied in detail [4–23]. The Jiaodong gold deposits formed between 123 and 110 Ma [24–32], much later than the formation of the Linglong granite (164–140 Ma; [6–8,10–12,18,25]) and immediately later than the formation of the Guojialing granite (135–125 Ma; [10,15,18,22]). The age of these gold deposits is consistent with previous age estimates of the Weideshan granite, which is associated with a few gold and many polymetallic deposits in the eastern Jiaodong Peninsula. It is worth noting that the only beryllium deposit in Jiaodong is produced in the Late Triassic Shidao granite [33]. Due to the small number and scale of polymetallic deposits, the research is not deep enough. However, almost every stage of magmatic activity has produced more or less polymetallic deposits since the Mesozoic. As a consequence, the relationship between the Mesozoic gold and polymetallic mineralization in Jiaodong Peninsula and tectonic evolution is unclear due to insufficient systematic research on regional magmatism, granite genesis, tectonic setting and its relationship with regional mineralization [15,34–39].

Methodical research on the origin of the above typical five-stage granites from Late Triassic to Early Cretaceous could significantly improve the general understanding of the tectonic setting and origin of gold and polymetallic mineralization. This paper is based on investigations into the composition, distribution, petrologic features, and published data of the typical five-stage granites, and presents a systematic study on morphology, geochemistry and geochronology of zircons from the granites, which elucidate associations between petrogenesis, tectonic setting, and gold and polymetallic mineralization. This study provides new insights into the relationship between magmatism and mineralization during the Mesozoic whilst also providing constraints on the tectonic setting of gold and polymetallic mineralization in the Jiaodong Peninsula.

2. Geological Background and Samples

East of the Tan–Lu fault, the study area is divided into the Sulu terrane in the southeast, the Jiaobei terrane in the northwest, and the Jiaolai basin in the middle. The two terranes are separated by the Wulian–Yantai fault in the east, which is commonly regarded as the boundary between the NCC and YC (Figure 1a). The Jiaobei terrane is bounded to the west by the Tan–Lu fault and to the east by the Wulian–Yantai fault, and contains both Precambrian metamorphic basement and Mesozoic magmatic rocks [40–45]. The Precambrian rocks in the Jiaobei terrane include the Neoarchean Jiaodong complex that consists of metamorphosed volcanic–sedimentary rocks and TTG (tonalite–trondhjemite–granodiorite) gneisses, as well as the Paleoproterozoic Jingshan and Fenzishan groups and the Neoproterozoic Penglai group, which consist of metasedimentary rocks [46]. The Paleoproterozoic Fenzishan group is the host rock of the gold and polymetallic deposits in Yantai city [47,48]. The Sulu terrane includes the Jiaonan terrane to the south and Weihai terrane to the north, and is part of the Qinling–Dabie–Sulu orogenic belt or the ultrahigh pressure (UHP) metamorphic belt of eastern central China [49–51] and represents an intercontinental collisional orogeny that evolved from the Permian to the Triassic [52–57]. The Jiaolai basin is a Cretaceous continental basin situated at the boundary between the Sulu terrane and Jiaobei terrane, and comprises volcanic–sedimentary rocks (Figure 1b).

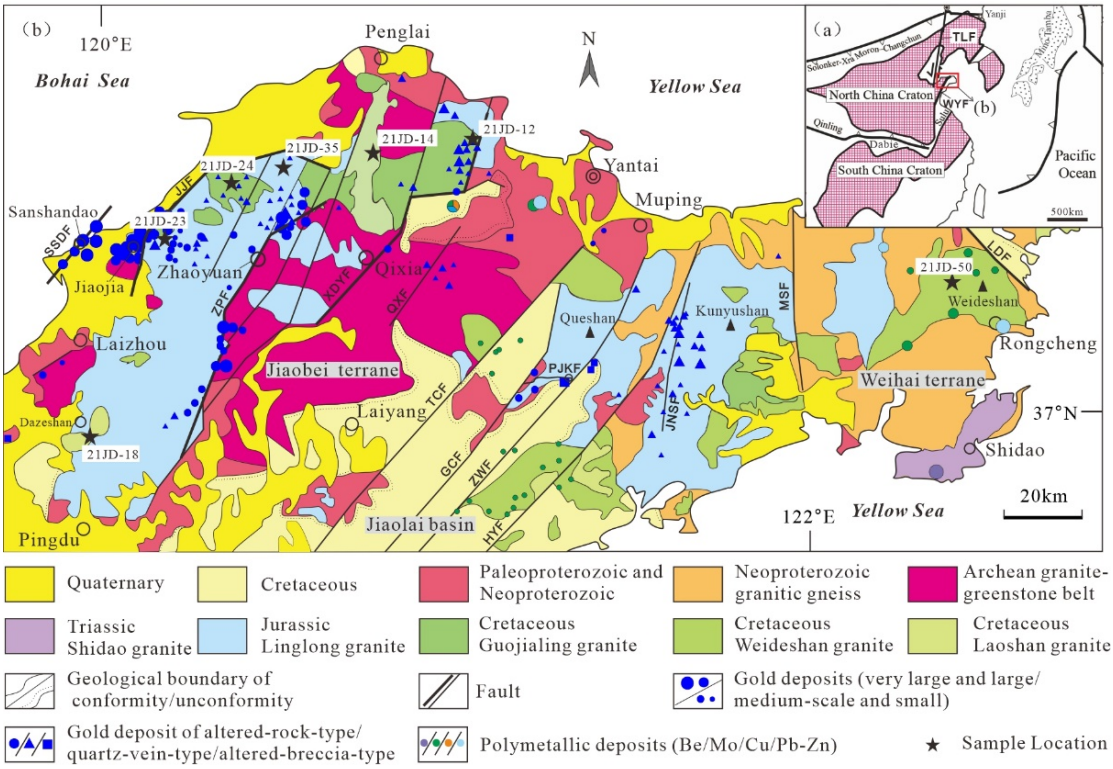

Figure 1. (**a**) Tectonic sketch map of east China, showing the location of the Jiaodong Peninsula. (**b**) Sketch map showing the regional geology and distribution of metal mineral deposits in the Jiaodong Peninsula (modified after [58,59]). Abbreviation: TLF = Tan–Lu fault zone; WYF = Wulian–Yantai fault zone; SSDF = Shanshandao fault zone; JJF = Jiaojia fault zone; ZPF = Zhaoyuan–Pingdu fault zone; XDYF = Xilin–Douya fault zone; QXF = Qixia fault zone; TCF = Taocun fault zone; GCF = Guocheng fault zone; ZWF = Zhuwu fault zone; HYF = Haiyang fault zone; PJKF = Pengjiakuang fault zone; JNSF = Jinniushan fault zone; MSF = Mishan fault zone; LDF = Lidao Fault zone.

Previous studies have shown that there is a concealed EW trending basement structure in the region, which is an anticlinorium and fault structure composed of Precambrian crystalline basement [60,61]. These basement structures are controlled by the regional tectonic stress domain of Mesozoic collision orogeny and subduction, and superimpose the fault tectonic system dominated by NE and NNE trending faults [60] (Figure 1b). Many faults are distributed on the upper wall of Tan–Lu fault from west to east, with the general trending from NE to nearly SN. These faults, which reach deep into the lower crust, are channels for the rise of deep magma, which not only affect the spatial location of regional magmatic rocks, but also control the formation and distribution of gold and polymetallic mineralization [33]. In addition, nearly EW- or NW-trending detachment faults developed at the northeast margin of Jiaolai basin, which controlled the distribution of deposits [62,63].

Besides the UHP metamorphic rocks, Mesozoic magmatic rocks are widely outcropped in the Jiaodong Peninsula (Figure 1b). They include the Triassic granite in the Shidao area, the widespread Jurassic–Cretaceous granites and the Cretaceous volcanic rocks in the Jiaolai Basin. Based on syn-magmatic evolution features, five main granitic types representing the five-stages of magmatism were defined [40]. The Jiaodong gold deposits mostly occur in the Linglong and Guojialing granites. No apparent gold mineralization exists in the Weideshan and Laoshan granites [58,64], although they have an affinity with the protolith age of the Weideshan granite [6,59,65,66]. However, all of the granites have different degrees of polymetallic mineralization.

3. Petrologic Features of the Typical Five–Stage Granites

This study focuses on the typical five-stage Mesozoic granites in the Jiaodong Peninsula. The Late Jurassic Linglong granite and Early Cretaceous Guojialing, Weideshan, and Laoshan granites are collected for analysis, and the sampling locations are shown in Figure 1b. At the same time, the published geochemical and geochronological data of the five-stage granites (including the Shidao granite) are collected for comprehensive study. Detailed geochemical data are listed in Supplementary Materials Tables S1 and S2.

3.1. The Late Triassic Shidao Granite

Late Triassic Shidao granite that intruded into the UHP granitic gneisses, covers an area of ~224 km^2, is located in the eastern UHP metamorphic belt (Figure 1b). The main lithology is composed of syenite with various structures (fine-, medium-, coarse-grained, and porphyritic), quartz syenite, and syenogranite, which together constitute the Shidao complex [40,67]. The former occupies about 40% of the total area of Shidao granite, while the latter occupy about 48% [68]. Scholars believe that syenogranite, the product of the rapid reentry after the collision between the YC and the NCC, is the source rock of Datuanliujia Be deposit, Rongcheng [2,33]. Previous studies on the chronology of the Shidao granite show that the zircon U–Pb, SHRIMP, and ^{40}Ar–^{39}Ar ages range from 227–200 Ma [69–74], suggesting that the main body of the Shidao granite was formed in the Late Triassic.

3.2. The Late Jurassic Linglong Granite

The Jurassic Linglong granite covers ~4230 km^2, and includes the Linglong pluton in the northwest Jiaodong Peninsula, as well as the Queshan and Kunyushan plutons between the Jiaobei and Weihai terranes. The main lithology is monzonitic granite. Predecessors suggested that the early intrusions were mainly gneissic garnet-bearing monzonitic granite, with later intrusions mainly being massive monzonitic granite [40,68]. The Linglong granite is the most developed granite in Jiaodong area and has always attracted much attention because of its distribution along with gold deposits. Therefore, some researchers call it one of the direct providers of ore–forming materials of Jiaodong gold deposit [75] or called it a derived source rock series [76,77]. However, the magmatic activity of this period has corresponding Mo–W polymetallic mineralization, for example, Xingjiashan Mo–W deposit is developed in Xingfushan pluton [2,78,79].

Two samples (21JD–23 and 21JD–35) are collected from Linglong pluton. Sample 21JD–23 (GPS: 37°23′27″ N, 120°10′20″ E) was collected from the abandoned quarry about 3 km east of Jiaojia gold deposit (Figure 1a). The main lithology is monzonitic granite [3]. The rock samples are light grayish white with medium- to coarse-grained texture and weak gneissic structure (Figure 2a). The main mineral composition is plagioclase (35 vol.%), K-feldspar (30 vol.%), quartz (30 vol.%) and biotite (5 vol.%). In addition, there are a few accessory minerals, such as garnet, zircon, titanite, etc. Sample 21JD–35 (GPS: 37°31′15″ N, 120°32′20″ E) is a monzonitic granite with a medium-grained texture, collected from the Longkou area, with a main mineral assemblage of K-feldspar (35 vol.%), plagioclase (30 vol.%), quartz (30 vol.%), and biotite (5 vol.%) (Figure 2b).

3.3. The Early Cretaceous Guojialing Granite

Outcrops of the Guojialing granite cover an area of ~514 km^2 in the northwest Jiaodong Peninsula. The Guojialing granite is discontinuously distributed, and the plutons, which roughly form a NEE-trending moniliform distribution (Figure 1b). The lithology is mainly porphyritic hornblende–bearing monzonitic granite, with minor granodiorite, quartz monzonite and monzodiorite [40,68]. Most of the gold deposits, especially the giant deposits, are genetically related to the Guojialing granite [2,75].

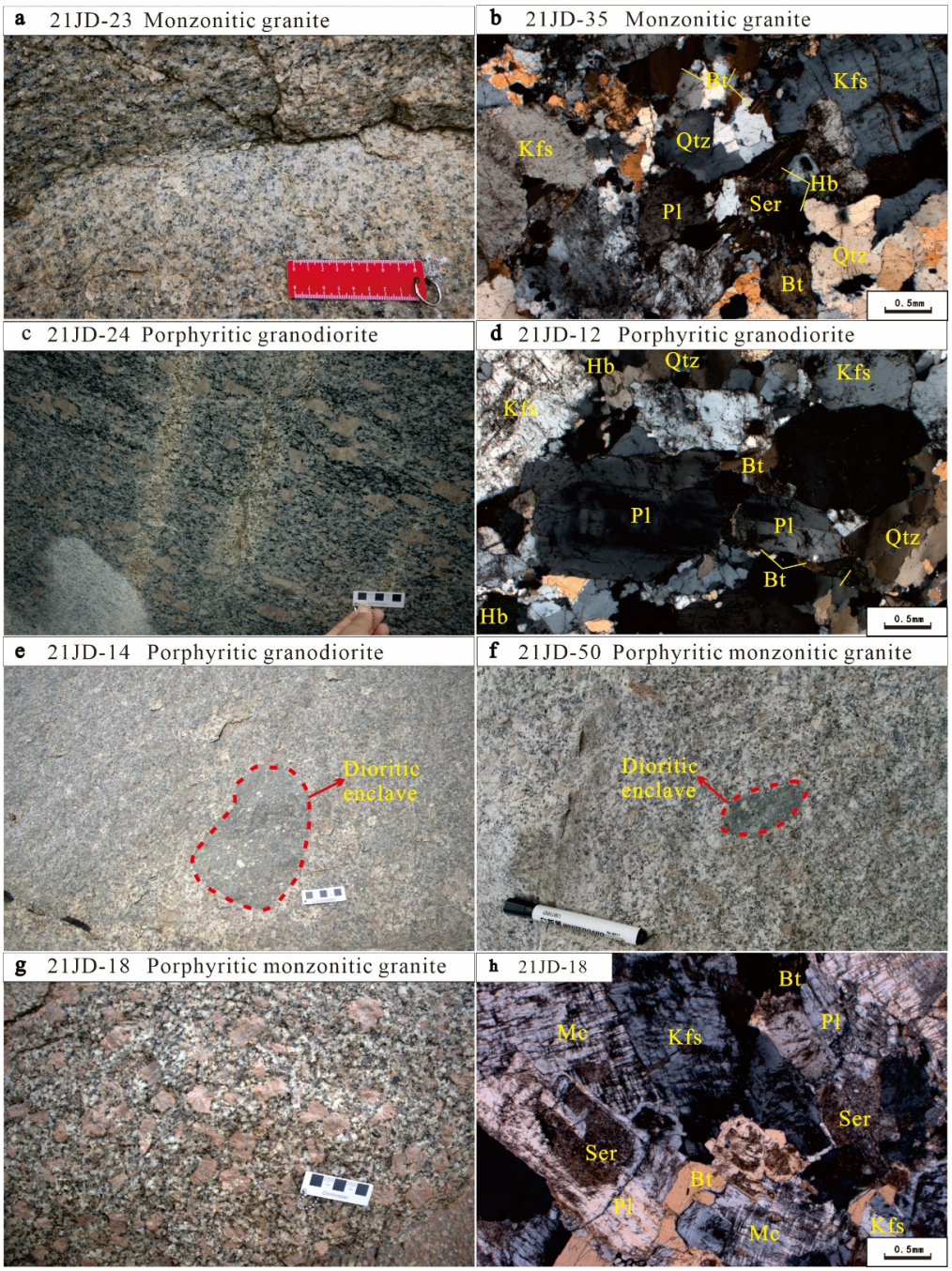

Figure 2. Field outcrop and photomicrographs (perpendicular polarized light) show textures and mineral assemblages of the Mesozoic granites in the Jiaodong Peninsula. (**a**,**b**) Monzonitic granite (Linglong granite samples 21JD–23 and 21JD–35); (**c**,**d**) porphyritic granodiorite (Guojialing granite samples 21JD–12 and 21JD–24); (**e**) porphyritic granodiorite (Weideshan granite sample 21JD–14); (**f**) porphyritic monzonitic granite (Weideshan granite sample 21JD–50); (**g**,**h**) porphyritic monzonitic granite (Laoshan granite sample 21JD–18). Abbreviation: Qtz = quartz; Pl = plagioclase; Kfs = K-feldspar; Bt = biotite; Hb = hornblende; Ser = sericite; Kln = kaoline; Mc = microcline.

Samples 21JD–12 and 21JD–24 were taken from Qujia and Guojialing plutons, respectively. Sample 21JD–12 (GPS: 37°37′38″ N, 121°03′54″ E) is a porphyritic granodiorite from the edge of the Guojialing pluton, Penglai City. It is grey in color with porphyraceous texture, and contains K-feldspar phenocrysts. The mineral assemblage comprises K-feldspar (40 vol.%), plagioclase (28 vol.%), quartz (20 vol.%), hornblende (6 vol.%), biotite

(5 vol.%), metallic minerals (1 vol.%), and minor apatite and titanite (Figure 3d). Sample 21JD–24 (GPS: 37°32′15″ N, 121°21′54″ E) is a porphyritic granodiorite from Qujia pluton, Zhaoyuan City. It is grey in color, and massive, with medium- to coarse-grained granitic texture (Figure 3c). The mineral assemblage includes K-feldspar (35 vol.%), plagioclase (25 vol.%), hornblende (20 vol.%), quartz (10 vol.%), biotite (5 vol.%), and minor secondary minerals (5 vol.% in total). Plagioclase and hornblende crystals are ~0.5–15 mm in length, with many dioritic enclaves visible in the hand specimen (Figure 2c).

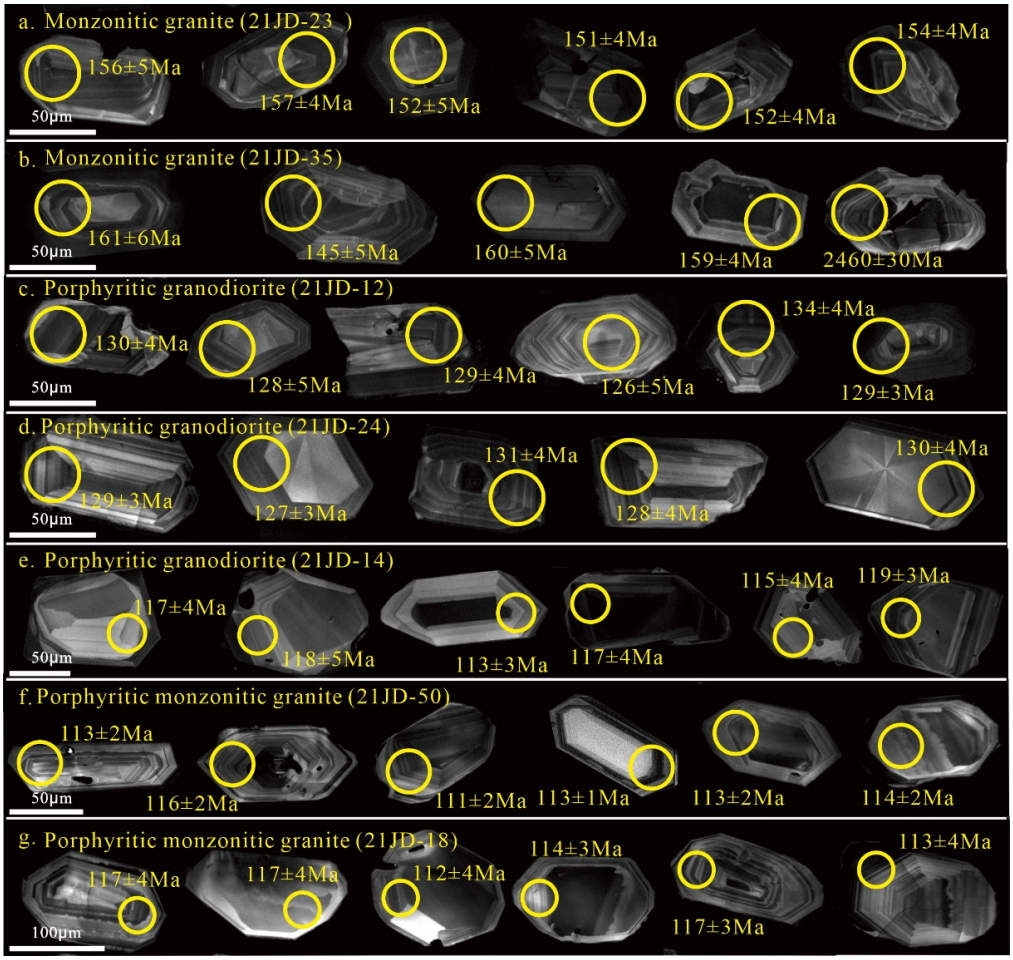

Figure 3. Representative zircon CL images for the Mesozoic granites in the Jiaodong Peninsula. Circles denote the analytical spots with LA–ICPMS zircon U–Pb ages. (**a**,**b**) Monzonitic granite (Linglong granite samples 21JD–23 and 21JD–35); (**c**,**d**) porphyritic granodiorite (Guojialing granite samples 21JD–12 and 21JD–24); (**e**) porphyritic granodiorite (Weideshan granite sample 21JD–14); (**f**) porphyritic monzonitic granite (Weideshan granite sample 21JD–50); (**g**) porphyritic monzonitic granite (Laoshan granite sample 21JD–18).

3.4. The Early Cretaceous Weideshan Granite

The Weideshan granite is dominated by quartz monzonite, monzonitic granite, and granodiorite [40]. Its outcrops cover ~2662 km^2 in the Jiaodong Peninsula, appearing as the large–scale Weideshan, Haiyang, and Jiaonan plutons in the Sulu orogenic belt, and as the smaller Aishan, Nansu, and Yashan plutons in the Jiaobei Terrane. The Weideshan granite is closely related to the regional contemporaneous Cu–Mo–Pb–Zn–Au polymetallic mineralization [2,3,65,77–79]. The magma that formed the Weideshan granite was derived from varying degrees of migmatization of mantle–crust source materials [3,6].

Sample 21JD–14 is a porphyritic granodiorite from the middle part of Aishan pluton (GPS: 37°31′10″ N, 121°44′10″ E), Penglai City. The sample is massive, with a porphyra-

ceous texture, and contains phenocrysts of K-feldspar (10~15 vol.%) in a medium- to fine-grained granitic groundmass (Figure 2e). The mineral assemblage includes plagioclase (40 vol.%), K-feldspar (25 vol.%), quartz (25 vol.%), hornblende (5 vol.%), biotite (3 vol.%), metallic minerals (2 vol.%), and minor apatite and titanite. Dioritic enclaves (5~20 cm diameter) are visible in hand specimen (Figure 2e). Sample 21JD–50 is a porphyritic monzonitic granite from the core of the Weideshan pluton (GPS: 37°17′16″ N, 122°18′59″ E), Rongcheng City. It is grey in color with porphyraceous texture, and contains K-feldspar phenocrysts (Figure 2f). It comprises plagioclase (35 vol.%), K-feldspar (30 vol.%), quartz (20 vol.%), hornblende (10 vol.%), biotite (4 vol.%), metallic minerals (1 vol.%), and minor apatite and titanite.

3.5. The Early Cretaceous Laoshan Granite

The Laoshan granite is mainly distributed in the southeast coastal area of Jiaodong Peninsula, and also sporadically distributed in the Dazeshan area of Jiaobei terrane, with a total area of ~1327 km^2. The rock assemblage here includes monzonitic granite, syenogranite, and alkali feldspar granite [22].

Sample 21JD–18 is a porphyritic monzonitic granite from the Dazeshan pluton (GPS: 37°01′10″ N, 119°57′25″ E), Pingdu city. It is massive with medium- to coarse-grained granitic texture, and contains dense K-feldspar phenocrysts (5 mm~4 cm in length, Figure 2g). The quartz miarolitic structure is well developed. The mineral assemblage includes K-feldspar (30 vol.%), plagioclase (30 vol.%), hornblende (15 vol.%), quartz (15 vol.%), biotite (8 vol.%), metallic minerals (1 vol.%), and minor secondary minerals (~1 vol.% in total) (Figure 2h).

4. Analytical Methods

4.1. Zircon Morphology

The pretreatment, mineral separation, target fabrication and Cathodoluminescence (CL) image shooting were all carried out at the Chengxin geological Testing Co., Ltd., Langfang, China. Zircon grains were separated by conventional magnetic and density techniques to concentrate the non-magnetic, heavy fractions. After sample preparation, zircon grains, free of visible inclusions and major fractures, were handpicked and embedded in epoxy resin and then polished to expose the grain centers. CL images were obtained using a JXA–8100 electron microprobe, in order to characterize the internal structure of the zircons and to select potential target sites for U–Pb analysis. Typical CL images are presented in Figure 3, together with the U–Pb ages for the corresponding spots.

4.2. Zircon U–Pb Dating and Trace Element Analyses

Zircon U–Pb dating and trace element analyses of zircons was conducted by LA–ICP–MS at the Guangzhou Tuoyan Analytical Technology Co., Ltd., Guangzhou, China. Laser sampling was performed using a NWR 193 laser ablation system. An iCAP RQ ICP–MS instrument was used to acquire ion–signal intensities. Helium was applied as a carrier gas. Argon was used as the make-up gas and mixed with the carrier gas via a Y-connector before entering the ICP. The spot size and frequency of the laser were set to 30 μm and 6 Hz, respectively, in this study. The energy was 3.5 J/cm^2. Zircon 91,500 [80] and glass NIST610 [81] were used as external standards for U–Pb dating and trace element calibration, respectively. Each analysis incorporated a background acquisition of approximately 30 s followed by 40 s of data acquisition from the sample. An Excel-based software ICPMSDataCal was used to perform off-line selection and integration of background and analyzed signals, time-drift correction and quantitative calibration for U–Pb dating and trace element analysis. $^{206}Pb/^{238}U$ and $^{207}Pb/^{206}Pb$ ages were interpreted to denote the crystallization ages of the <1000 Ma and >1000 Ma zircon grains, respectively. The results for isotopic ratios, calculated ages and key trace element compositions are listed in Table 1.

Table 1. Summary of key REE, U–Pb isotopic data of magmatic zircons from the Mesozoic granites in the Jiaodong Peninsula, China.

No.	REE		Th/U	Isotopic Ratio						Apparent Age (Ma)					
	Eu/Eu*	Ce/Ce*		$^{207}Pb/^{206}Pb$	1σ	$^{207}Pb/^{235}U$	1σ	$^{206}Pb/^{238}U$	1σ	$^{207}Pb/^{206}Pb$	1σ	$^{207}Pb/^{235}U$	1σ	$^{206}Pb/^{238}U$	1σ
Linglong granite sample 21JD–23															
21JD-23-01	0.10	11.36	0.25	0.1261	0.0027	6.3926	0.1644	0.3678	0.0091	2044	38	2031	23	2019	43
21JD-23-02	0.24	71.24	0.52	0.0488	0.0043	0.1648	0.0143	0.0245	0.0008	136	194	155	12	156	5
21JD-23-03	0.36	42.11	0.41	0.0490	0.0024	0.1662	0.0083	0.0246	0.0007	149	111	156	7	157	4
21JD-23-04	0.44	7.49	0.87	0.0491	0.0049	0.1613	0.0158	0.0239	0.0008	151	216	152	14	152	5
21JD-23-05	0.41	42.83	0.36	0.0534	0.0062	0.1775	0.0203	0.0241	0.0009	345	244	166	18	154	5
21JD-23-06	0.17	24.11	0.32	0.0489	0.0024	0.1650	0.0081	0.0245	0.0007	143	109	155	7	156	4
21JD-23-07	0.44	69.92	0.65	0.0483	0.0132	0.1544	0.0415	0.0232	0.0015	112	545	146	36	148	10
21JD-23-08	0.32	17.11	0.62	0.0536	0.0043	0.1622	0.0129	0.0220	0.0007	352	171	153	11	140	4
21JD-23-09	0.43	146.71	0.15	0.0514	0.0029	0.1679	0.0096	0.0237	0.0007	260	124	158	8	151	4
21JD-23-10	0.31	37.52	0.57	0.0531	0.0115	0.1776	0.0376	0.0243	0.0013	332	428	166	32	155	8
21JD-23-11	0.45	8.32	0.89	0.0522	0.0058	0.1811	0.0199	0.0252	0.0009	294	236	169	17	160	6
21JD-23-12	0.50	81.46	0.59	0.0494	0.0093	0.1671	0.0308	0.0245	0.0012	167	389	157	27	156	7
21JD-23-13	0.35	36.21	0.62	0.0474	0.0057	0.1660	0.0195	0.0254	0.0009	70	262	156	17	162	6
21JD-23-14	0.13	26.62	0.45	0.1479	0.0037	8.3151	0.2364	0.4078	0.0104	2322	42	2266	26	2205	48
21JD-23-15	0.49	45.15	0.98	0.0526	0.0060	0.1733	0.0194	0.0239	0.0009	310	240	162	17	152	5
21JD-23-16	0.36	4.78	0.32	0.0493	0.0039	0.1708	0.0134	0.0251	0.0008	164	175	160	12	160	5
21JD-23-17	0.14	122.00	0.19	0.1544	0.0039	8.9175	0.2541	0.4190	0.0107	2395	42	2330	26	2256	49
21JD-23-18	0.08	144.16	0.19	0.0488	0.0027	0.1639	0.0093	0.0244	0.0007	136	126	154	8	155	4
21JD-23-19	0.29	15.17	0.33	0.0517	0.0030	0.1697	0.0099	0.0238	0.0007	271	128	159	9	152	4
21JD-23-20	0.23	69.33	0.32	0.0498	0.0035	0.1658	0.0117	0.0241	0.0007	186	157	156	10	154	4
Linglong granite sample 21JD-35															
21JD-35-01	0.79	2.28	0.17	0.0618	0.0095	0.2120	0.0316	0.0253	0.0010	667	299	195	26	161	6
21JD-35-02	0.29	11.75	0.17	0.0815	0.0068	1.7931	0.1448	0.1634	0.0047	1233	155	1043	53	976	26
21JD-35-03	0.40	57.29	0.18	0.0427	0.0098	0.1819	0.0409	0.0314	0.0015	0	305	170	35	200	10
21JD-35-04	0.34	166.97	0.18	0.1757	0.0081	8.8279	0.3896	0.3727	0.0090	2613	74	2320	40	2042	42
21JD-35-05	0.52	247.13	0.57	0.0808	0.0139	1.9159	0.1192	0.1753	0.0033	1217	306	1035	71	1056	20
21JD-35-06	0.29	252.58	0.55	0.0524	0.0069	0.1609	0.0207	0.0228	0.0007	303	276	152	18	145	5
21JD-35-07	0.50	29.19	0.88	0.0533	0.0112	0.1856	0.0382	0.0256	0.0013	343	418	173	33	163	8
21JD-35-08	0.26	6.14	0.14	0.0652	0.0157	0.2565	0.0598	0.0291	0.0018	782	438	232	48	185	11
21JD-35-09	0.51	31.98	0.14	0.1741	0.0059	10.2746	0.3306	0.4342	0.0072	2597	56	2460	30	2325	32
21JD-35-10	0.40	131.25	0.15	0.1526	0.0064	6.2519	0.2513	0.3026	0.0061	2376	70	2012	35	1704	30
21JD-35-11	0.10	1.72	0.44	0.0568	0.0068	0.1946	0.0226	0.0252	0.0007	481	245	181	19	160	5
21JD-35-12	0.71	17.95	0.33	0.0617	0.0057	0.2107	0.0190	0.0250	0.0006	665	188	194	16	159	4
21JD-35-13	0.20	26.82	0.51	0.0563	0.0096	0.1640	0.0271	0.0214	0.0008	462	338	154	24	136	5
21JD-35-14	0.81	1.91	0.09	0.0703	0.0061	1.8682	0.0733	0.1606	0.0023	936	170	915	40	968	23
21JD-35-15	0.84	1.33	0.20	0.0517	0.0096	0.1473	0.0266	0.0208	0.0008	270	377	140	24	132	5
21JD-35-16	0.49	14.86	0.79	0.0424	0.0095	0.1771	0.0390	0.0306	0.0014	0	279	166	34	194	9
21JD-35-17	0.38	137.06	0.12	0.1978	0.0286	10.6834	0.3718	0.4765	0.1838	2608	219	2341	36	2564	58

Table 1. *Cont.*

No.	REE		Th/U	Isotopic Ratio						Apparent Age (Ma)					
	Eu/Eu*	Ce/Ce*		$^{207}Pb/^{206}Pb$	1σ	$^{207}Pb/^{235}U$	1σ	$^{206}Pb/^{238}U$	1σ	$^{207}Pb/^{206}Pb$	1σ	$^{207}Pb/^{235}U$	1σ	$^{206}Pb/^{238}U$	1σ
21JD-35-18	0.56	16.61	0.79	0.0768	0.0169	0.2475	0.0526	0.0235	0.0013	1116	386	225	43	150	8
21JD-35-19	2.47	1.32	0.02	0.1181	0.0115	3.7234	0.3493	0.2295	0.0080	1928	165	1576	75	1332	42
21JD-35-20	0.12	96.34	0.04	0.2090	0.0093	16.8560	0.7084	0.5878	0.0120	2898	70	2927	40	2981	49
Guojialing granite sample 21JD-12															
21JD-12-01	0.43	6.71	0.63	0.0475	0.0100	0.1354	0.0279	0.0207	0.0011	75	435	129	25	132	7
21JD-12-02	0.41	78.84	0.53	0.0514	0.0033	0.1445	0.0094	0.0204	0.0006	259	142	137	8	130	4
21JD-12-03	0.47	49.35	0.41	0.0663	0.0050	0.2272	0.0169	0.0249	0.0008	815	149	208	14	158	5
21JD-12-04	0.62	1.32	0.62	0.0474	0.0028	0.1335	0.0078	0.0204	0.0006	68	133	127	7	130	4
21JD-12-05	0.32	47.84	0.17	0.0495	0.0057	0.1431	0.0164	0.0210	0.0007	172	250	136	15	134	5
21JD-12-06	0.50	2.07	0.65	0.0522	0.0028	0.1464	0.0080	0.0204	0.0006	293	118	139	7	130	4
21JD-12-07	0.49	9.64	0.60	0.0489	0.0073	0.1351	0.0199	0.0200	0.0008	144	317	129	18	128	5
21JD-12-08	0.46	111.40	0.52	0.1713	0.0082	10.7043	0.5267	0.4531	0.0150	2571	78	2498	46	2409	66
21JD-12-09	0.46	15.13	0.58	0.0496	0.0046	0.1366	0.0126	0.0200	0.0006	177	204	130	11	128	4
21JD-12-10	0.49	4.98	0.31	0.0487	0.0061	0.1420	0.0175	0.0212	0.0008	132	270	135	16	135	5
21JD-12-11	0.42	56.98	0.66	0.1584	0.0056	7.0552	0.2641	0.3230	0.0091	2439	58	2118	33	1804	44
21JD-12-12	0.55	1.71	0.55	0.0509	0.0058	0.1505	0.0169	0.0215	0.0008	235	243	142	15	137	5
21JD-12-13	0.72	7.01	0.53	0.1801	0.0063	10.3570	0.3889	0.4170	0.0121	2654	57	2467	35	2247	55
21JD-12-14	0.23	59.32	0.51	0.0490	0.0036	0.1361	0.0099	0.0202	0.0006	147	163	130	9	129	4
21JD-12-15	0.54	86.87	0.63	0.0489	0.0070	0.1331	0.0187	0.0198	0.0008	141	305	127	17	126	5
21JD-12-16	0.48	62.31	0.55	0.0490	0.0046	0.1416	0.0131	0.0210	0.0007	147	206	135	12	134	4
21JD-12-17	0.66	9.81	0.63	0.0489	0.0043	0.1424	0.0125	0.0211	0.0007	141	195	135	11	135	4
21JD-12-18	0.44	189.91	0.58	0.0531	0.0026	0.1485	0.0074	0.0203	0.0006	333	106	141	7	129	3
21JD-12-19	0.45	190.16	0.48	0.0491	0.0066	0.1433	0.0188	0.0212	0.0008	154	285	136	17	135	5
21JD-12-20	0.51	117.60	0.51	0.0477	0.0142	0.1271	0.0370	0.0193	0.0013	82	586	121	33	123	8
Guojialing granite sample 21JD-24															
21JD-24-01	0.61	89.13	0.64	0.0468	0.0021	0.1305	0.0061	0.0202	0.0005	37	105	125	5	129	3
21JD-24-02	0.64	354.87	0.47	0.0482	0.0025	0.1365	0.0072	0.0206	0.0006	108	118	130	6	131	3
21JD-24-03	0.53	111.08	0.62	0.0477	0.0050	0.1370	0.0143	0.0209	0.0007	82	233	130	13	133	4
21JD-24-04	0.60	93.98	0.61	0.0486	0.0024	0.1387	0.0071	0.0207	0.0006	127	114	132	6	132	4
21JD-24-05	0.50	66.09	0.78	0.0489	0.0024	0.1347	0.0068	0.0200	0.0005	144	111	128	6	127	3
21JD-24-06	0.57	242.67	0.31	0.0476	0.0080	0.1384	0.0227	0.0211	0.0009	79	356	132	20	135	6
21JD-24-07	0.56	110.01	0.71	0.0483	0.0029	0.1362	0.0083	0.0205	0.0006	112	137	130	7	131	4
21JD-24-08	0.59	253.94	0.71	0.0487	0.0027	0.1368	0.0077	0.0204	0.0006	135	125	130	7	130	4
21JD-24-09	0.50	136.14	0.58	0.0507	0.0032	0.1402	0.0088	0.0201	0.0006	226	138	133	8	128	4
21JD-24-10	0.57	77.41	0.63	0.0521	0.0059	0.1396	0.0156	0.0194	0.0007	291	240	133	14	124	4
21JD-24-11	0.58	142.38	0.89	0.0492	0.0025	0.1386	0.0072	0.0204	0.0006	157	115	132	6	130	3
21JD-24-12	0.57	122.35	0.62	0.0489	0.0027	0.1385	0.0078	0.0206	0.0006	141	126	132	7	131	4
21JD-24-13	0.56	207.60	0.57	0.0488	0.0026	0.1390	0.0074	0.0207	0.0006	139	119	132	7	132	4
21JD-24-14	0.54	57.24	0.72	0.0487	0.0098	0.1405	0.0277	0.0209	0.0011	133	415	134	25	134	7

Table 1. *Cont.*

No.	REE		Th/U	Isotopic Ratio						Apparent Age (Ma)					
	Eu/Eu*	Ce/Ce*		$^{207}Pb/^{206}Pb$	1σ	$^{207}Pb/^{235}U$	1σ	$^{206}Pb/^{238}U$	1σ	$^{207}Pb/^{206}Pb$	1σ	$^{207}Pb/^{235}U$	1σ	$^{206}Pb/^{238}U$	1σ
21JD-24-15	0.56	173.35	0.69	0.0458	0.0020	0.1292	0.0059	0.0205	0.0005	0	88	123	5	131	3
21JD-24-16	0.51	154.94	0.83	0.0507	0.0026	0.1376	0.0072	0.0197	0.0005	226	114	131	6	126	3
21JD-24-17	0.55	126.05	0.56	0.0497	0.0033	0.1394	0.0094	0.0203	0.0006	182	149	133	8	130	4
21JD-24-18	0.64	89.58	0.62	0.0490	0.0034	0.1341	0.0093	0.0199	0.0006	146	155	128	8	127	4
21JD-24-19	0.63	58.36	0.80	0.0474	0.0035	0.1366	0.0102	0.0209	0.0006	70	169	130	9	133	4
21JD-24-20	0.53	69.71	0.70	0.0502	0.0026	0.1441	0.0076	0.0208	0.0006	205	115	137	7	133	4
Weideshan granite sample 21JD-14															
21JD-14-01	0.50	82.10	1.03	0.0487	0.0094	0.1179	0.0224	0.0176	0.0009	133	401	113	20	112	5
21JD-14-02	0.57	34.24	1.12	0.0503	0.0047	0.1267	0.0118	0.0183	0.0006	210	205	121	11	117	4
21JD-14-03	0.43	43.44	1.11	0.0520	0.0067	0.1316	0.0166	0.0183	0.0007	287	270	126	15	117	4
21JD-14-04	0.61	56.34	1.36	0.0529	0.0055	0.1329	0.0136	0.0182	0.0006	323	218	127	12	117	4
21JD-14-05	0.48	2.31	0.92	0.1745	0.0058	0.5906	0.0208	0.0246	0.0007	2601	54	471	13	156	4
21JD-14-06	0.53	112.87	1.13	0.0493	0.0077	0.1255	0.0192	0.0184	0.0008	164	328	120	17	118	5
21JD-14-07	0.50	9.63	1.42	0.0492	0.0036	0.1273	0.0093	0.0188	0.0006	159	163	122	8	120	3
21JD-14-08	0.55	1.69	0.86	0.0483	0.0035	0.1180	0.0087	0.0177	0.0005	112	165	113	8	113	3
21JD-14-09	0.55	109.46	0.95	0.0510	0.0048	0.1291	0.0119	0.0184	0.0006	242	201	123	11	117	4
21JD-14-10	0.54	2.00	0.85	0.0490	0.0066	0.1208	0.0159	0.0179	0.0007	149	286	116	14	114	4
21JD-14-11	0.46	1.57	1.13	0.0527	0.0037	0.1352	0.0095	0.0186	0.0006	317	152	129	9	119	3
21JD-14-12	0.53	3.05	0.87	0.0512	0.0052	0.1275	0.0127	0.0181	0.0006	251	217	122	11	115	4
21JD-14-13	0.37	132.84	0.83	0.0485	0.0036	0.1257	0.0092	0.0188	0.0006	123	164	120	8	120	4
21JD-14-14	0.58	17.92	1.36	0.0500	0.0041	0.1296	0.0105	0.0188	0.0006	196	179	124	9	120	4
21JD-14-15	0.56	50.91	0.99	0.0500	0.0136	0.1240	0.0331	0.0180	0.0012	197	534	119	30	115	7
21JD-14-16	0.34	25.10	1.04	0.0507	0.0033	0.1316	0.0087	0.0188	0.0005	228	145	126	8	120	3
21JD-14-17	0.68	15.46	1.06	0.0518	0.0037	0.1324	0.0095	0.0186	0.0006	276	156	126	8	119	3
21JD-14-18	0.53	1.51	0.98	0.0508	0.0059	0.1395	0.0160	0.0199	0.0007	233	248	133	14	127	5
21JD-14-19	0.54	118.13	0.84	0.0488	0.0043	0.1270	0.0110	0.0189	0.0006	138	193	121	10	121	4
21JD-14-20	0.54	61.00	1.16	0.0511	0.0147	0.1347	0.0379	0.0191	0.0013	244	555	128	34	122	8
Weideshan granite sample 21JD-50															
21JD-50-01	0.51	81.79	0.69	0.0468	0.0035	0.1133	0.0083	0.0176	0.0003	39	174	109	8	113	2
21JD-50-02	0.35	112.64	0.86	0.0522	0.0032	0.1221	0.0073	0.0170	0.0002	295	139	117	7	109	1
21JD-50-03	0.46	168.41	0.68	0.0460	0.0032	0.1145	0.0081	0.0181	0.0003	110	92	110	7	116	2
21JD-50-04	0.35	196.71	0.74	0.0529	0.0036	0.1218	0.0076	0.0168	0.0003	324	156	117	7	107	2
21JD-50-05	0.35	65.87	0.89	0.0501	0.0023	0.1208	0.0053	0.0175	0.0002	211	101	116	5	112	1
21JD-50-06	0.33	162.18	0.81	0.0524	0.0027	0.1232	0.0062	0.0171	0.0002	306	117	118	6	109	1
21JD-50-07	0.33	160.43	0.87	0.0481	0.0019	0.1148	0.0046	0.0173	0.0002	106	91	110	4	110	1
21JD-50-08	0.28	127.50	0.74	0.0491	0.0037	0.1174	0.0092	0.0174	0.0003	154	170	113	8	111	2
21JD-50-09	0.46	10.59	1.42	0.0531	0.0025	0.1099	0.0047	0.0151	0.0002	345	103	106	4	97	2
21JD-50-10	0.35	2.39	0.84	0.0505	0.0023	0.1196	0.0053	0.0172	0.0002	217	106	115	5	110	1
21JD-50-11	0.58	90.86	0.71	0.0531	0.0033	0.1234	0.0073	0.0171	0.0003	345	145	118	7	109	2

Table 1. *Cont.*

No.	REE		Th/U	Isotopic Ratio						Apparent Age (Ma)					
	Eu/Eu*	Ce/Ce*		$^{207}Pb/^{206}Pb$	1σ	$^{207}Pb/^{235}U$	1σ	$^{206}Pb/^{238}U$	1σ	$^{207}Pb/^{206}Pb$	1σ	$^{207}Pb/^{235}U$	1σ	$^{206}Pb/^{238}U$	1σ
21JD-50-12	0.31	142.77	1.02	0.0470	0.0021	0.1132	0.0052	0.0174	0.0001	56	98	109	5	112	1
21JD-50-13	0.30	160.79	0.93	0.0493	0.0023	0.1204	0.0058	0.0176	0.0002	161	105	115	5	113	1
21JD-50-14	0.40	145.41	0.83	0.0500	0.0029	0.1216	0.0066	0.0177	0.0002	195	133	116	6	113	1
21JD-50-15	0.38	98.65	0.99	0.0522	0.0021	0.1268	0.0050	0.0176	0.0002	295	86	121	4	113	2
21JD-50-16	0.33	33.64	1.20	0.0486	0.0034	0.1168	0.0075	0.0177	0.0002	128	159	112	7	113	1
21JD-50-17	0.31	148.21	0.81	0.0475	0.0019	0.1125	0.0046	0.0172	0.0002	76	93	108	4	110	1
21JD-50-18	0.33	194.22	0.78	0.0462	0.0019	0.1110	0.0045	0.0175	0.0002	6	96	107	4	112	1
21JD-50-19	0.45	64.82	0.80	0.0485	0.0036	0.1180	0.0085	0.0178	0.0003	124	176	113	8	114	2
21JD-50-20	0.35	156.23	0.82	0.0470	0.0024	0.1127	0.0055	0.0175	0.0002	50	119	108	5	112	2
21JD-50-21	0.32	140.88	0.74	0.0505	0.0022	0.1219	0.0055	0.0175	0.0002	220	99	117	5	112	1
21JD-50-22	0.38	14.28	1.01	0.0511	0.0022	0.1216	0.0054	0.0172	0.0002	256	98	117	5	110	1
21JD-50-23	0.36	138.41	0.78	0.0490	0.0020	0.1165	0.0047	0.0173	0.0002	146	94	112	4	111	1
21JD-50-24	0.41	121.86	0.79	0.0508	0.0022	0.1214	0.0052	0.0174	0.0002	232	100	116	5	111	1
21JD-50-25	0.30	129.74	0.80	0.0487	0.0022	0.1169	0.0052	0.0175	0.0002	200	103	112	5	112	1
Laoshan granite sample 21JD-18															
21JD-18-01	0.50	3.69	1.02	0.0485	0.0047	0.1227	0.0117	0.0183	0.0006	125	212	118	11	117	4
21JD-18-02	0.54	15.69	1.27	0.0485	0.0030	0.1252	0.0077	0.0187	0.0005	123	137	120	7	120	3
21JD-18-03	0.53	34.34	1.01	0.0490	0.0044	0.1242	0.0110	0.0184	0.0006	149	196	119	10	117	4
21JD-18-04	0.39	3.32	0.89	0.0512	0.0042	0.1303	0.0097	0.0187	0.0003	250	186	124	9	119	2
21JD-18-05	0.47	4.01	0.91	0.0501	0.0031	0.1290	0.0083	0.0187	0.0003	198	144	123	7	115	2
21JD-18-06	0.20	11.18	0.54	0.0514	0.0027	0.1298	0.0071	0.0183	0.0005	256	118	124	6	117	3
21JD-18-07	0.48	4.06	0.61	0.0483	0.0018	0.1333	0.0054	0.0200	0.0005	115	87	127	5	128	3
21JD-18-08	0.24	72.56	0.49	0.0491	0.0049	0.1236	0.0121	0.0182	0.0006	154	216	118	11	117	4
21JD-18-09	0.39	63.42	1.02	0.0531	0.0065	0.1285	0.0155	0.0176	0.0007	332	256	123	14	112	4
21JD-18-10	0.48	26.74	1.05	0.0482	0.0038	0.1213	0.0096	0.0183	0.0006	109	177	116	9	117	4
21JD-18-11	0.43	3.32	0.83	0.0488	0.0041	0.1204	0.0100	0.0179	0.0006	138	184	116	9	114	4
21JD-18-12	0.42	7.35	0.52	0.0505	0.0047	0.1326	0.0105	0.0194	0.0005	220	200	126	9	118	3
21JD-18-13	0.41	161.66	0.71	0.0503	0.0047	0.1275	0.0109	0.0188	0.0005	209	200	122	10	120	3
21JD-18-14	0.32	75.21	0.65	0.0509	0.0036	0.1339	0.0086	0.0192	0.0003	235	163	128	8	118	2
21JD-18-15	0.54	7.56	0.70	0.0486	0.0023	0.1197	0.0059	0.0179	0.0005	126	108	115	5	114	3
21JD-18-16	0.16	5.47	0.48	0.0460	0.0047	0.1216	0.0124	0.0192	0.0006	0	227	117	11	123	4
21JD-18-17	0.39	149.88	0.98	0.0493	0.0044	0.1242	0.0111	0.0183	0.0006	160	197	119	10	117	4
21JD-18-18	0.23	2.34	0.52	0.0480	0.0038	0.1209	0.0091	0.0184	0.0003	102	178	116	8	110	2
21JD-18-19	0.41	55.26	0.68	0.0521	0.0060	0.1159	0.0132	0.0162	0.0006	288	243	111	12	103	4
21JD-18-20	0.37	92.09	0.77	0.0527	0.0058	0.1282	0.0139	0.0177	0.0006	314	233	123	13	113	4

Errors are 1-sigma. $Eu/Eu^* = 2 \times Eu_N/(Sm_N + Gd_N)$, represents the degree of Eu anomaly. $Ce/Ce^* = 2 \times Ce_N/(La_N + Pr_N)$, represents the degree of Ce anomaly.

5. Results

Seven representative samples of the Mesozoic granites including monzonitic granite (samples 21JD–23 and 21JD–35) of Linglong granite, porphyritic granodiorite (samples 21JD–12 and 21JD–24) of Guojialing granite, porphyritic granodiorite (sample 21JD–14) and porphyritic monzonitic granite (sample 21JD–50) of Weideshan granite, and porphyritic monzonitic granite (sample 21JD–18) from Laoshan granite were selected for zircon U–Pb dating. Zircon U–Pb geochronology and geochemistry data are summarized in Table 1. Errors on individual analyses are cited as 1σ, and the weighted mean $^{206}Pb/^{238}U$ ages are quoted at the 95% confidence level. CL images of the representative zircon grains with $^{206}Pb/^{238}U$ ages are shown in Figure 3.

5.1. The Linglong Granite

Zircons in the monzonitic granite (sample 21JD–23) are subhedral to euhedral (Figure 3a). CL imaging reveals that most grains are prismatic, colorless, transparent, and ranging from 50 to 150 μm in length, as well as show concentric oscillatory zoning (Figure 3a). In addition, the chondrite-normalized REE patterns are strongly enriched in heavy rare earth elements (HREEs) and depleted in light rare earth element (LREEs, Figure 4b). The zircons have strong negative Eu anomalies (Eu/Eu* = 0.08–0.50), high Ce/Ce* ratios (Ce/Ce* = 4.78–84.16, some reaching 146.71) and high Th/U ratios (0.15–0.98), characteristic of magmatic zircon (Table 1, [82–84]). Twenty zircon grains were analyzed for U–Pb isotopes. Except for three inherited grains yielding $^{207}Pb/^{206}Pb$ ages from 2395 ± 42 Ma to 2044 ± 38 Ma, the remaining seventeen concordant analyses yield apparent $^{206}Pb/^{238}U$ ages ranging from 162 ± 6 Ma to 140 ± 4 Ma with a weighted mean of 154 ± 2 Ma (MSWD = 1; n = 17) ($^{206}Pb/^{238}U$ and $^{207}Pb/^{206}Pb$ ages that were interpreted to denote the crystallization ages of the <1000 Ma and >1000 Ma zircon grains, respectively) (Figure 4a). The latter age can be considered as crystallization age of the granite, and is consistent with the zircon U–Pb ages of 164–140 Ma previously reported [85–87]. The Neoproterozoic zircon ages with normal magmatic zircon features indicate that the protolith rocks were not completely remelted, representing the information of magma source area, that is, derived from the Precambrian basement of NCC and subduction plate of YC.

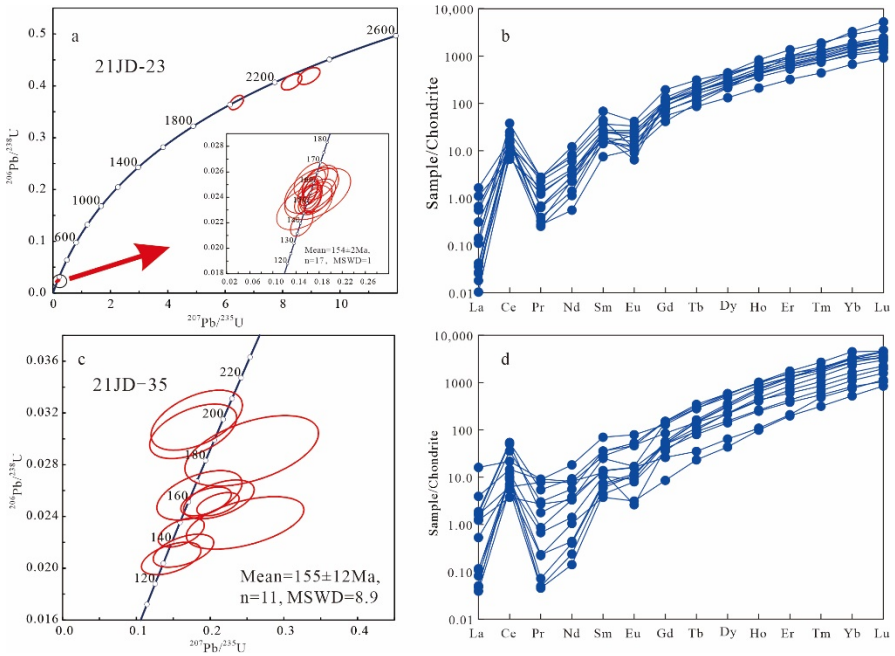

Figure 4. Samples from the Late Jurassic Linglong granite. (**a**,**c**) LA–ICP–MS magmatic zircon U–Pb concordia diagrams and dating results of samples 21JD–23 and 21JD–35, respectively. (**b**,**d**) Chondrite–normalized REE patterns of zircons from samples 21JD–23 and 21JD–35, respectively.

Zircons in the monzonitic granite (sample 21JD–35) are also euhedral, prismatic, colorless, and transparent. They range from 100 to 300 μm in size with length/width ratios of 1:1 to 3:1. CL imaging reveals that most grains have fine oscillatory growth zones (Figure 3b). All zircons have similar chondrite–normalized REE patterns, strongly enriched in HREEs and depleted in LREEs (Figure 4d), but with a slightly flatter HREE profile than the sample 21JD–35. Their strongly negative Eu anomalies (Eu/Eu* = 0.10–0.84, with one zircon grain recording a higher Eu/Eu* ratio of 2.47), high Ce/Ce* ratios (Ce/Ce* = 1.32–252.58) and high Th/U ratios (0.02–0.88) are characteristic of magmatic zircon (Table 1, [82–84]). Twenty zircon grains were analyzed for U–Pb isotopes. Eleven age-spots on zircons yield concordant $^{206}Pb/^{238}U$ ages ranging from 200 ± 10 Ma to 132 ± 5 Ma with a weighted mean of 155 ± 12 Ma (MSWD = 8.9; *n* = 11) (Figure 4c). This age can be considered as crystallization age of the granite, and is similar to the zircon U–Pb age (154 ± 2 Ma, Figure 4a) of the sample 21JD–35. Meanwhile, this sample has more Proterozoic–Archaeozoic ages than the former. It is probably that the sample location is closer to the edge of the pluton, resulting in more xenoliths and incomplete melting components of the NCC and YC.

5.2. The Guojialing Granite

Zircons in the porphyritic granodiorite (samples 21JD–12 and 21JD–24) are subhedral to euhedral and range from 100 to 300 μm in size. CL imaging reveals that most grains have fine oscillatory growth zones (Figure 3c,d). All zircons have similar chondrite-normalized REE patterns, strongly enriched in HREEs and depleted in LREEs (Figure 5b,d). Their strongly negative Eu anomalies (Eu/Eu* = 0.23–0.72), high Ce/Ce* ratios (Ce/Ce* = 1.32–354.87, most are less than 100) and high Th/U ratios (0.17–0.89) are characteristic of magmatic zircon (Table 1, [82–84]).

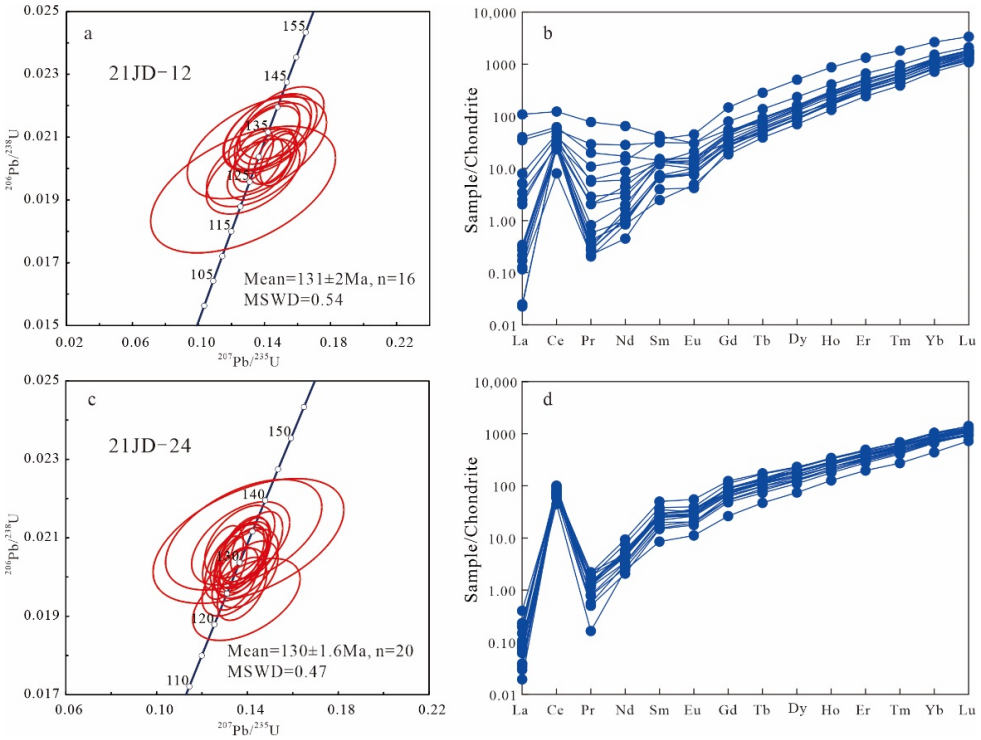

Figure 5. Samples from the Early Cretaceous Guojialing granite. (**a**,**c**) LA–ICP–MS magmatic zircon U–Pb concordia diagrams and dating results of samples 21JD–12 and 21JD–24, respectively. (**b**,**d**) Chondrite–normalized REE patterns of zircons from samples 21JD–12 and 21JD–24, respectively.

Twenty zircon grains from porphyritic granodiorite (sample 21JD–12) were analyzed for U–Pb isotopes, of which one analysis (21JD–12–03) was excluded because of high discordance caused by cracks within the zircons. Except for three inherited grains yielding

$^{207}Pb/^{206}Pb$ ages from 2439 ± 58 Ma to 2570 ± 78 Ma, the remaining sixteen age-spots on zircons yield concordant $^{206}Pb/^{238}U$ ages ranging from 137 ± 5 Ma to 123 ± 8 Ma with a weighted mean of 131 ± 2 Ma (MSWD = 0.54; *n* = 16) (Figure 5a). This age can be considered as crystallization age of the granite. There are also twenty zircon grains from porphyritic granodiorite (sample 21JD–24) were analyzed for U–Pb isotopes. Twenty age-spots on zircons yield concordant $^{206}Pb/^{238}U$ ages ranging from 135 ± 6 Ma to 124 ± 4 Ma with a weighted mean of 130 ± 2 Ma (MSWD = 0.47; *n* = 20) (Figure 5c). These ages are consistent with the zircon U–Pb ages of 135–125 Ma previously reported by [85–87].

5.3. The Weideshan Granite

Zircons in the porphyritic granodiorite (sample 21JD–14) and porphyritic monzonitic granite (sample 21JD–50) are euhedral and range from 150 to 300 μm in size. CL imaging reveals that most grains have fine oscillatory growth zones (Figure 3e,f). All zircons have similar chondrite-normalized REE patterns, strongly enriched in HREEs and depleted in LREEs (Figure 6b,d). Their strongly negative Eu anomalies (Eu/Eu* = 0.28–0.68, averaged at 0.44), high Ce/Ce* ratios (Ce/Ce* = 1.51–196.71, averaged at 83.35) and high Th/U ratios (0.68–1.42, averaged at 0.95) are characteristic of magmatic zircon (Table 1, [82–84]).

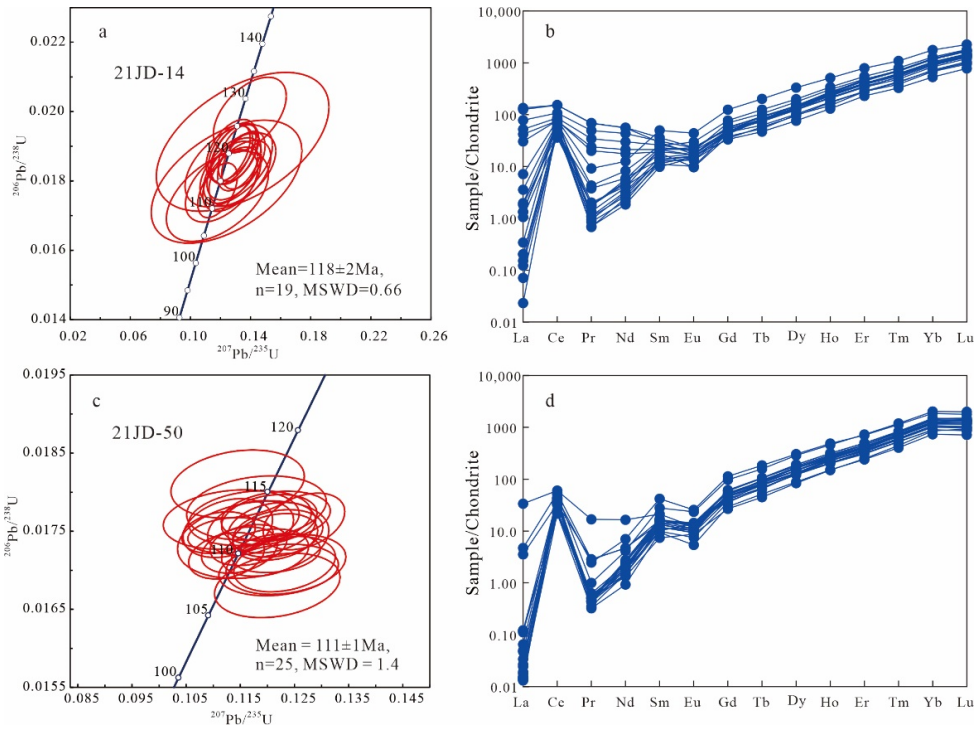

Figure 6. Samples from the Early Cretaceous Weideshan granite. (**a**,**c**) LA–ICP–MS magmatic zircon U–Pb concordia diagrams and dating results of samples 21JD–14 and 21JD–50, respectively. (**b**,**d**) Chondrite–normalized REE patterns of zircons from samples 21JD–14 and 21JD–50, respectively.

Twenty zircon grains from porphyritic granodiorite (sample 21JD–14) were analyzed for U–Pb isotopes, of which one analysis (21JD–14–05) was excluded due to being far from the concordant curve, possibly due to the presence of mineral inclusions. The remaining nineteen age–spots on zircons yield concordant $^{206}Pb/^{238}U$ ages ranging from 112 ± 5 Ma to 127 ± 5 Ma with a weighted mean of 118 ± 2 Ma (MSWD = 0.66; *n* = 19) (Figure 6a). This age can be considered as crystallization age of the granite. There are also twenty-five zircon grains from porphyritic monzonitic granite (sample 21JD–50) that were analyzed for U–Pb isotopes. All age-spots on zircons yield concordant $^{206}Pb/^{238}U$ ages ranging from 97 ± 2 Ma to 116 ± 2 Ma with a weighted mean of 111 ± 1 Ma (MSWD = 1.4; *n* = 25) (Figure 6c). These ages are consistent with the zircon U–Pb ages of 125–110 Ma previously reported by [85–87].

5.4. The Laoshan Granite

Zircons in the porphyritic monzonitic granite (sample 21JD–18) are also euhedral, prismatic, colorless, and transparent. They are granular, ranging from 80 to 300 μm in size, with aspect ratios of 1:1.5 to 4:1. CL imaging reveals that most grains have fine oscillatory growth zones (Figure 3g). All zircons have similar chondrite-normalized REE patterns, strongly enriched in HREEs and depleted in LREEs (Figure 7b). Their strongly negative Eu anomalies (Eu/Eu* = 0.16–0.54, averaged at 0.40), high Ce/Ce* ratios (Ce/Ce* = 2.34–161.66, averaged at 39.96) and high Th/U ratios (0.48–1.27, averaged at 0.78) are characteristic of magmatic zircon (Table 1, [82–84]). Of the twenty zircons from the porphyritic monzonitic granite (sample 21JD–18) that were dated by LA-ICP-MS U–Pb analysis, yield concordant $^{206}Pb/^{238}U$ ages ranging from 103 ± 4 Ma to 120 ± 3 Ma with a weighted mean of 116 ± 2 Ma (MSWD = 0.043; *n* = 20) (Figure 7a).

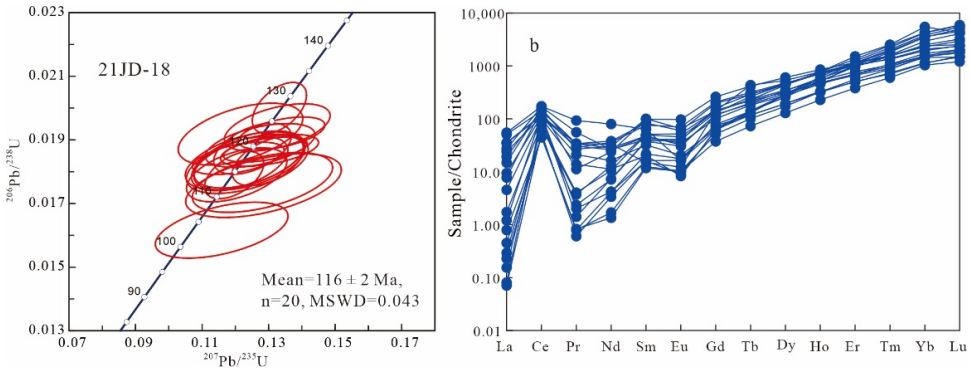

Figure 7. Samples from the Early Cretaceous Laoshan granite. (**a**) LA–ICP–MS magmatic zircon U–Pb concordia diagrams and dating results of sample 21JD–18. (**b**) Chondrite–normalized REE patterns of zircons from sample 21JD–18.

6. Discussion

6.1. Magma Sources and Petrogenesis of Granites

6.1.1. The Triassic Shidao Granite

The Shidao granite is the only one that has been reported with a Late Triassic age in the Weihai terrane. The isotopic age of Shidao granite tested by predecessors is ranging from 227 to 200 Ma [69–74].

The Shidao granite is composed of syenite, quartz syenite, and syenogranite from early to late. The only Be deposit in the Jiaodong area is found in Shidao syenogranite (205.7 ± 1.4 Ma, [72]). The Shidao granite intruded into the UHP metamorphic rocks in the Sulu orogenic belt, indicating that they were formed after the UHP metamorphic event. Many isotopic ages of eclogites in the Sulu orogenic belt have been measured by previous studies, and the results are as follows: 228–221 Ma (Sm–Nd method) [88,89], 217.1 ± 8.7 Ma (U–Pb method) [90], and 228 ± 29 Ma (zircon SHRIMP method) [91]. The zircon isotopic ages of cores and edges of UHP coesite-bearing gneiss with SHRIMP method, which were 242–209 Ma and 230–202 Ma, respectively, suggesting that 242–224 Ma were UHP metamorphic ages and 229–202 Ma were UHP retrograde metamorphic ages [92,93]. It can be seen that the formation age of Shidao granite is consistent with the retrograde metamorphism age of UHP metamorphic rocks or the roll back timing of UHP metamorphic rocks [69]. Previous studies suggest that the Shidao granite is a syn-orogenic (syn-reentry) intrusive rock that related to plate segment dissociation during the subduction of the YC and NCC [71,72,94] or post-orogenic intrusive rock [70,73,74]. In this study, we agree with the latter, that the Shidao alkaline rocks were generated under a post-collisional extensional setting. In view of the hornblende facies at the retrograde metamorphism stage of the UHP metamorphic rocks, it is considered that the Shidao granite is the product of partial melting of enriched lithospheric mantle, crystallization differentiation, and assimilation mixing of lower crust under the condition of UHP metamorphic rocks returning to hornblende facies.

6.1.2. The Jurassic–Cretaceous Granites

The Jurassic–Cretaceous intrusive rocks are well developed in the Jiaodong Peninsula, mainly including Linglong, Guojialing, Weideshan, and Laoshan granites. Previous studies have carried out a large number of isotopic tests on Late Mesozoic magmatic rocks. Some scholars have calculated the age data of Jurassic–Cretaceous granites with high accuracy by using different testing methods [95]. The diagenetic ages of the four-stage granites are approximately 164–140 Ma, 135–125 Ma, 125–110 Ma, and 120–104 Ma, respectively [6–8,10–12,15,18,22,25,30,31,65,66,72,96–106]. The data obtained in this paper are basically in line with the previous chronological data.

The Linglong granite is the main ore-hosting body of Jiaodong gold deposit. According to statistics, about 77% of Jiaodong gold deposits and a large porphyry Mo deposit (e.g., Xingjiashan, molybdenite Re–Os method, 158.7 ± 2.5 Ma) occur in the Linglong granite [107]. The Linglong granite is composed of monzogranite series intrusive rocks. The $^{87}Sr/^{86}Sr$, εNd (t), εHf(t) and Sr/Y values of Linglong granite are 0.711281~0.712418, −21.6~−19.4, −28.7~6.2, and 55.07~214.44, respectively. εHf (t) values are placed at 1.9 and 2.5 Ga crustal evolution lines [18,108]. The low εHf (t) value, high Sr/Y value and no obvious negative Eu anomaly of the rock are similar to adakite [9,18], which is similar to Jiaodong Neoarchean TTG [109]. At the same time, the Linglong granite often contains peraluminous minerals such as garnet, which indicates S–type granite feature. Magma was formed in a relatively high-pressure environment and was derived from partial melting of the thickened lower crust of North China [16]. The ages of the Linglong granite range from 164 to 140 Ma, which should be considered as the major period of magma crystallization [11,12,15,18,31,72,97,99,100,102,103]. Simultaneously, the development of a large number of inherited zircons indicates the complexity of the origin of Linglong granite, which are products of partial melting of Neoarchean crystalline basement in the NCC and remnants of deep subduction materials in the Sulu UHP metamorphic belt.

The Guojialing granite is predominantly distributed in Jiaodong gold concentration area, and is an important ore-hosting body of Jiaodong gold deposit. About 10% of the gold deposits occur in the Guojialing granite [107]. This stage of granite is closely related to Jiaodong gold deposit due to its closely metallogenic timing and spatial distribution. The Guojialing granite is an intrusive rock series composed of monzodiorite, adamellite, granodiorite, and monzonitic granite, with the I-type granite and adakite geochemical features of crust–mantle mixed sources [85,86]. The Guojialing granite is rich in Neoarchean and Paleoproterozoic inherited zircons, with a few of Jurassic, but no Neoproterozoic and early Paleozoic inherited zircons [18]. It implies that the crust source material is the Precambrian basement of NCC, and Sulu orogenic belt and YC materials are missing. At present, researchers agree on the genesis of the Guojialing granite, which is believed to be the result of the mixing of the lower crust acidic magma formed by partial melting of the Jiaodong basement metamorphic rock series and mantle-derived basic magma [85,86]. The formation of the magma is related to the subduction of the PPP beneath the NCC and the upwelling of the asthenosphere. The scholars have systematically tested the isotopic age of the Guojialing granite by various dating methods. The results show that the isotopic ages range from 132 to 125 Ma, and the host rocks are consistent with the age of the dioritic enclaves, indicating simultaneous emplacement of both acid and basic magmas [7,8,10,12,15,18,104,106].

The Weideshan granite has a certain spatial distance with gold mineralization, but they are closely related to Cu, Pb, Zn and Mo deposits [3,65,110]. The Weideshan granite is composed of rocks with an independent evolutionary history and protolith origin, different from the Linglong, Guojialing, and Laoshan granites. The Weideshan granite displays similarities in lithofacies and geochemistry with the Guojialing granite. However, the Guojialing granite has similarities in trace element composition with adakite, tonalite-trondhjemite-granodiorite, and sodic granite, while the Weideshan granite closely resembles typical island arc rocks [111,112]. The Guojialing and Weideshan granites typically contain microgranular dioritic enclaves with mantle-like geochemical characteristics [6,21,113]. The geochemical characteristics imply that the Weideshan granite is a blend of crust–mantle de-

rived magma, and the magma is derived from partial melting of recycled continental crust material and enriched lithospheric mantle [85,86,114]. Zircon U–Pb ages of the Weideshan granite range from 120 to 107 Ma [85]. The age of dioritic enclaves is moderately younger than that of host rocks, indicating the basic magma is earlier than the emplacement of acidic magma. It is hard to see ancient inherited zircons in the rocks, demonstrating that there was no surrounding rock material blended in the process of magma emplacement.

The Laoshan granite is predominantly distributed in the UHP metamorphic belt in the east and south of the Jiaodong gold concentration area, but there is no direct spatial distribution relationship with gold mineralization and nonferrous metal mineralization. The Laoshan granite is composed of monzonitic granite, syenogranite, and alkali–feldspar granite, which transited from acidic to alkaline, with uneven distribution of miarolitic structure [22]. Geochemical characteristics show that Laoshan granite is an A-type granite formed in regional extensional tectonic background, resulting from the Mesozoic lithosphere thinning and craton destruction [114]. The magma derived from partial melting of the deep crust, which may be related to the back–arc extensional setting.

A comprehensive analysis of available data for this area reveals that from Jurassic to Early Cretaceous, the geochemical composition of four-stage granites evolved from high-potassium calc–alkaline series to peridotite series, from peraluminous to metaluminous, trace element contents change from high Ba–Sr to low Ba–Sr and from high Sr, low Y to low Sr and high Y, REE composition change from no or weak positive Eu anomaly to significant negative Eu anomaly, the granite-type evolved from S-type through I-type to A-type. It shows that the mantle beneath the Jiaodong Peninsula evolved from EM–II in the Jurassic to EM–I in the Early Cretaceous, with depleted mantle emerging in the Late Cretaceous [18,40,110,115,116]. This demonstrates that the mantle switched from enriched to depleted [86,110].

6.2. Tectonic Setting

A large number of studies have disclosed that the genetic type of granites not only reflects the nature of magma source area, but is also a discriminant mark of tectonic environment of magma formation [117–119]. A-type granites are widely regarded as important petrological markers of extensional environment, but differences in environment, scale, and depth frequently lead to different characteristics of A–type granites [120]. Consequently, further studies divided A-type granites into A_1 and A_2 types, in which A_1 type granite comprises mantle-derived melt discrete crystalline rocks, predominantly formed in anorogenic environments (continental rifts or intraplate stretching) [117]. A_2 type granites represent rocks of crustal partial melting origin, predominantly formed in post-orogenic environment [121]. A-type granites were formed in an extensional environment under the background of crustal extension and thinning, and are closely related to the post-collision orogeny [122–127]. The nature and degree of crustal extension background is one of the critical factors that inhibit the formation of A-type granites and affect the characteristics of magma and emplacement. Consequently, the determination of A-type granite has become an important petrological marker to differentiate the tectonic environment of continental crust extension, and the end time and location of orogenesis [117,128–133].

Previous in-depth studies on the Shidao granite indicated that the materials were derived from the enriched lithosphere mantle source area, and were intrusive rocks with different compositions due to different stages of melting and experiencing different degrees of crystallization differentiation and assimilation and mixing of the lower crust [74]. In the diagram of geochemical composition classification, the sample are plot in in the A-type granite area (Figure 8). In the Nb–Y–3Ga trigonometric projection map, A_2 granite area was more invested than A_1 granite area (Figure 9a). In the tectonic discrimination diagrams, the Shidao granite is mostly plot in the within-plate granite (WPG) area, and a small amount is plot in the volcanic arc granite (VAG) area (Figure 9b,c). In R_1–R_2 diagram, samples fall into the border zone of late orogenic and anorogenic (Figure 9d), shows the Shidao granite is formed in the tectonic environment transition period. The existence of UHP metamorphic rocks represented by eclogites in Sulu orogenic belt indicates that the belt underwent continental deep subduction,

continental collision, and rapid exhumation of UHP metamorphic rocks in NCC and YC during the mid-late Triassic (Figure 10a). The occurrence of Shidao A-type granite marks the end of the strong collisional orogeny and the structural reentry of UHP metamorphic rocks in the Sulu orogenic belt, and the transition from the NCC–YC tectonic system to the Paleo–Pacific tectonic system in Jiaodong area [134].

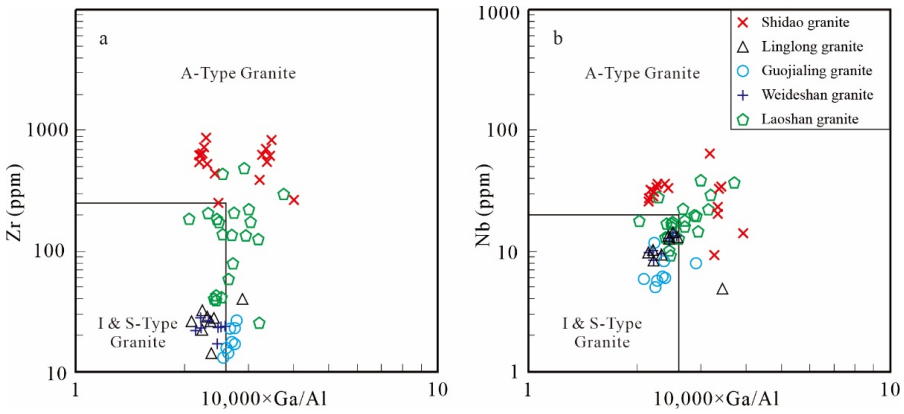

Figure 8. (**a**) Zr and (**b**) Nb versus 10,000 × Ga/Al discrimination diagrams showing the genetic types of granites (Base map after [135], data for the Linglong, Guojialing and Weideshan granites are from [86]; data for the Laoshan and Shidao granites are from [86,133] and [70,73,74], respectively). Detailed geochemical data are listed in Supplementary Materials Table S1.

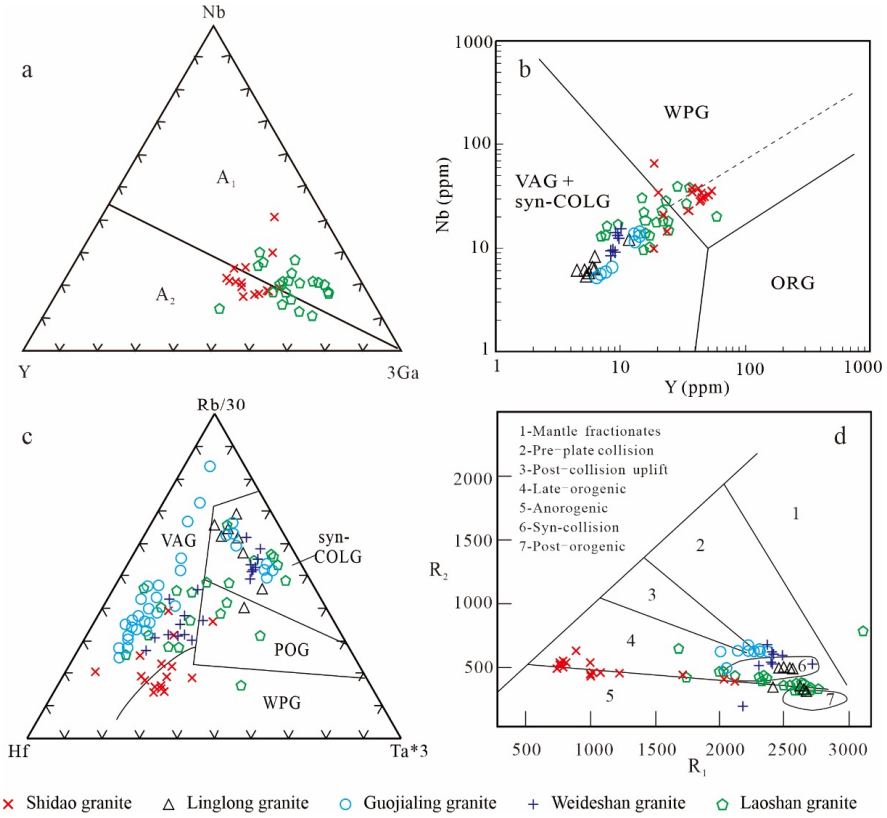

Figure 9. Tectonic discrimination diagrams for the Mesozoic granites in the Jiaodong Peninsula (Base map after [136,137]); the Shidao granite data of (**a**–**c**) is quoted from [70,73,74]; data of Laoshan granite in the figure are quoted from [86,133]; some data of d is from [106,112]); the Linglong, Guojialing, and Weideshan granites' data of (**b**–**d**) are quoted from [86,112]. Detailed geochemical data are listed in Supplementary Materials Tables S1 and S2. Abbreviations: VAG = volcanic arc granite, ORG = ocean ridge granite, WPG = within-plate granite, Syn-COLG = syn-collisional granite.

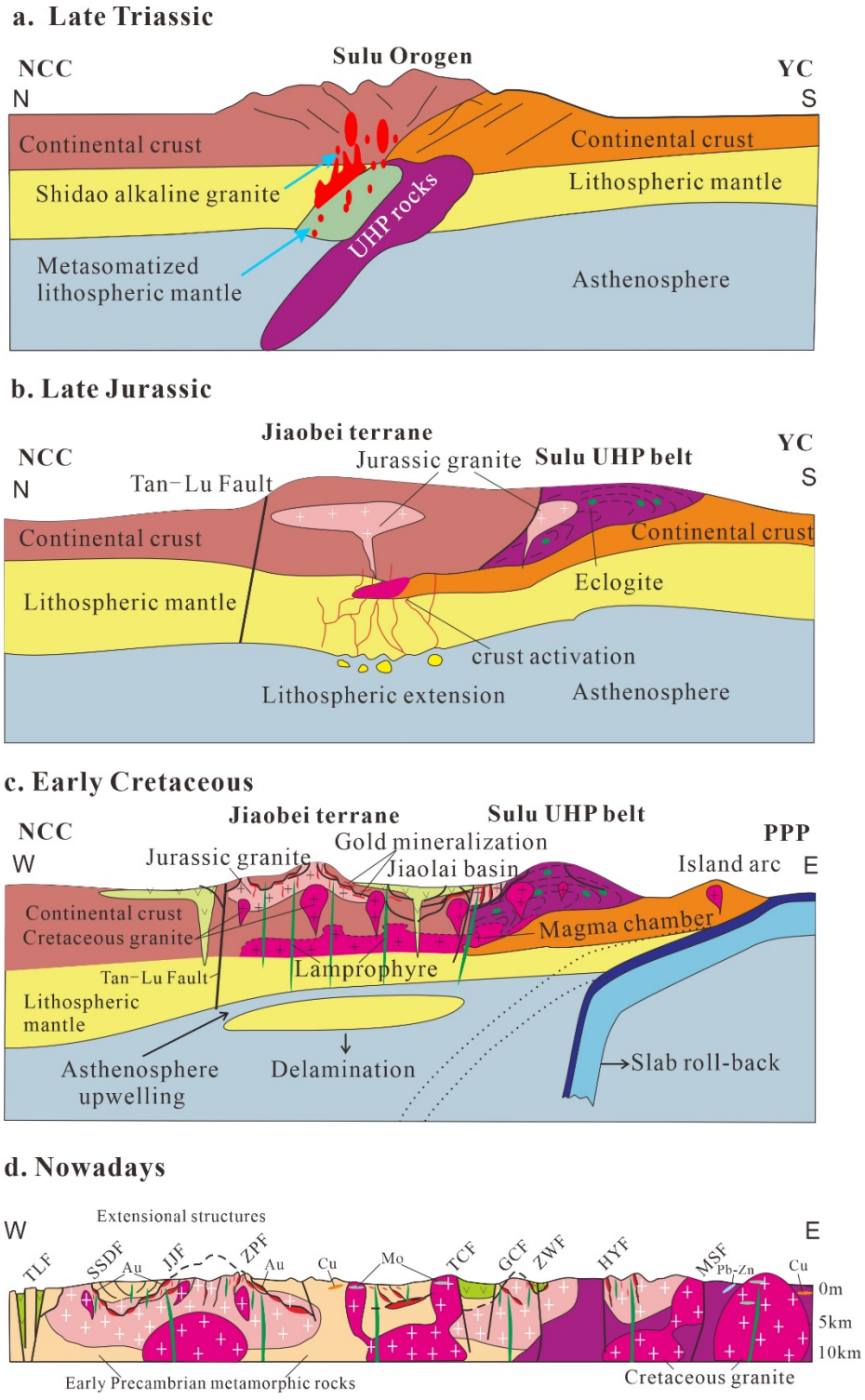

Figure 10. Schematic diagrams showing Mesozoic geodynamic evolution in the Jiaodong Peninsula, China (modified after [18,58,73,138,139]). (**a**) Partial melting of the metasomatic mantle wedge, generating the Shidao arc-like alkaline complex; (**b**) Since the Late Jurassic, the thickened crust experienced gravitational collapse under relatively high-pressure conditions, resulting in in-situ remelting of the thickened continental crust to form the crust-derived Linglong granite; (**c**) The crustal thickening event reached its peak during the early Cretaceous and the delamination of the modified lithosphere initiated a strong crust–mantle interaction, forming crust–mantle-derived mixed magma and I-type Guojialing and Weideshan granites and gold deposits; (**d**) The magma evolved along the upwelling process of the fault and formed a series of polymetallic deposits.

The tectonic setting of Linglong granite has syn- to post-collision characteristics (Figure 9c,d), and the S–type granite features and the ubiquitous gneissic phenomenon indicate that the granite was in a compressional state during diagenesis. In R_1–R_2 diagram (Figure 9d), the Linglong and Guojialing granites fall into the range of syn-collisional to post-collisional/late orogenic granite, respectively, revealing their tectonic background transformed from compression to extension. The Weideshan granite exhibits the characteristics of arc or syn-collisional granite in terms of geochemistry [86], indicating that it was formed on the volcanic arc that suffered a tectonic compression (Figure 9; [58,86]). The geological occurrence analysis indicates that the Laoshan granite is closely associated with the Weideshan granite, forming an I–A type composite granitic pluton. During the formation of the Weideshan granite, magma from the partial remelting of crustal rocks did not obviously mix with mantle-derived magma, but instead formed the A–type Laoshan granite [40,86,89]. The Laoshan granite samples are distributed in the A_1–A_2 region of the Nb–Y–3Ga triangulation map (Figure 9a). The mineral composition of Laoshan granite shows that the early unit is A_2-type granite dominated by syenogranite, and the late unit is A_1-type alkali feldspar granite that often containing the alkaline dark minerals such as sodium amphibole and aegirine. In the discriminant diagram of tectonic environment, most of the samples are plotted in the volcanic arc to collisional granite area and the volcanic arc area (Figure 9b,c), illustrating the geochemical information of the arc magmatism. In the R_1–R_2 diagram, most of the samples fall into the boundary of late-orogenic, anorogenic, and post-orogenic region (Figure 9d), but one situated in mantle fractionates indicates mantle contribution during the diagenetic process [137]. Together with related calc–alkaline granites, the Laoshan granite reveal the evolution process of late Mesozoic craton destruction and are important indicators after the peak of NCC destruction.

6.3. The Relationship between Tectonic Movement, Magmatic Activity, and Gold and Polymetallic Mineralization

Mesozoic magmatism in the Jiaodong Peninsula reflects the entire evolution of geodynamics in the Mesozoic, indicating the switch from NCC−YC collision to subduction of the PPP, with crustal thickening switching to lithospheric thinning, and a compressional tectonic setting changing to an extensional setting alternately. The superposition and transformation of the tectonic system is closely related to the formation and temporal–spatial distribution of gold and polymetallic mineralization. It can be concluded that the Late Triassic–Early Cretaceous magmatism in the Jiaodong Peninsula experienced four peaks in the Late Triassic, Late Jurassic, early and late period of the Early Cretaceous (Figure 10).

The subduction of the YC beneath the NCC resulted in continent–continent collision and HP/UHP metamorphism in the Late Triassic (Figure 10a). UHP metamorphic eclogites with ages of 240–200 Ma are widespread in the east of Jiaodong Peninsula [140]. Due to the break-off of eclogitized oceanic lithosphere at the transition zone of the continental and oceanic lithospheres, the subducted continental lithosphere ceased further descend and was rising with buoyancy. The exhumation of the deeply subducted continental crust resulted in decompression dehydration and partial melting of the UHP metamorphic slices to generate aqueous felsic melts. The felsic melts reacted with the overlying mantle wedge to cause a metasomatized mantle (Figure 10a). Partial melting of the metasomatic mantle wedge could generate post-collisional arc-like magmatism (i.e., the Shidao alkaline granite; 227–200 Ma) (Figure 10a). The alkaline magmatism experienced a successive fractional crystallization process. In the process of ascending and migrating along the fault in the late magmatic evolution, the residual magma rich in Be, as Han and Ma [141] suggested, mixed with a CO_2-rich fluid and large amount of atmospheric water. The addition of acidic fluid changed the earlier alkaline environment, destroyed the lattice balance, and precipitated a large amount of Be. Be element is wrapped in alteration minerals such as sericite in the form of bertrandite ($Be_4[Si_2O_7](OH)_2$), thus forming Be orebody, namely Datuanliujia Be deposit [33].

Since the Late Jurassic (180–170 Ma), with the rapid and low-angle subduction of the PPP along the NW direction to eastern China, the crust in the Jiaodong Peninsula has been continuously thickened [140,142,143] (Figure 10b). The peninsula experienced gravitational collapse under relatively high-pressure conditions, resulting in in-situ remelting of the thickened continental crust to form the crust-derived Linglong granite (164–140 Ma) (Figure 10b). Its sources include the orogenic belt subduction material and the NCC's lower crust. It implies that the formation processes of the granite was influenced by the NCC and YC [18,100,144]. The S-type granitic magma and the homologous magma rose along the deep fault and form the plutons and dikes. The ore-bearing gas and liquid produced in the process of magmatic condensation diffused to the surrounding rock along the fault. Extensive skarn and skarn–type Mo–W mineralization are formed in the contact zone. The hydrothermal vein W–Mo mineralization and polymetallic mineralization are mainly formed in the structural fracture zone and detachment belt far away from the contact zone, and molybdenum ore bodies that mainly formed in the later hydrothermal vein mineralization occurred in the pluton [2].

The early period of the Cretaceous was mainly influenced by the westward subduction of the PPP, with the compressional tectonic system switching to one of extension and the lithosphere responding to intense back–arc extension [38,100]. The YC merged with the NCC completely in the early Cretaceous, and the crustal thickening event reached its peak during this period. As a result, delamination of the modified lithosphere initiated a strong crust–mantle interaction, forming crust–mantle-derived mixed magma and I-type Guojialing granite and Weideshan granite (135–110 Ma; Figure 10c). The magma evolved along the upwelling process of the fault and formed the hydrothermal fluid rich in ore-forming materials, which metasomatized with the surrounding rock or at the top of the pluton in appropriate places. The ore-forming materials were further precipitated and enriched, forming a series of porphyry–skarn-type polymetallic deposits such as the Xiangkuang Cu–Pb–Zn deposit and Wangjiazhuang Cu–Zn deposit (Figure 10d).

The swift subduction of the Paleo–Pacific crust in the NWW direction and the subsequent slab roll-back resulted in strong mantle convection, intensified lithospheric delamination, and asthenospheric upwelling during the late period of the Early Cretaceous [139,145]. Underplating by rising magma caused the partial melting of the lower crust, generating large-scale crust–mantle-derived magma and forming the K-rich Weideshan granite (Figure 10). It directly leads to intense magmatism, rapid upwelling of magma, and a series of extensional structures in the Jiaodong Peninsula. Geologists have termed it "thermal upwelling–extension" [85]. The extensive gold and polymetallic mineralization in the Jiaodong Peninsula displays close affinity with these thermal upwelling–extension structures. Acting as a "heat generator", magmatic activity activated ore-bearing fluid in the surrounding rocks and lead to migration of ore-bearing fluid from the mantle to the upper crust to aid its mineralization. The fractured system generated by extension, related to magma upwelling, providing space for the Jiaodong gold deposits [146]. In the middle and late period of magmatic differentiation of Weideshan stage, a large amount of ore-bearing hydrothermal fluid gathered, and the shift of external temperature and pressure and the opening of space led to the immiscibility and boiling of fluid. Meanwhile, the mixing of different fluids and the water–rock reaction led to the shift of pH value and composition of the fluid, which led to the precipitation and mineralization of Cu and Mo minerals in the favorable parts of the structure. In the late stage of magmatic evolution, the surrounding groundwater circulates in a wide range driven by magmatic heat, and the crustal ore-forming materials are extracted, which migrate, enrich, and precipitate along the fault zone, forming the middle–low temperature hydrothermal vein type Pb–Zn–Ag–Au polymetallic mineralization in the late stage of magmatic intrusion. During this period, the porphyry Cu–Mo polymetallic deposits such as Lengjia, Shangjiazhuang, and Nantai were formed (Figure 10d).

According to the formation age of the deposit, scholars believe that there are three major ore-forming periods in Jiaodong area corresponding to the three major magma stages.

That is, the Indosinian polymetallic mineralization period corresponding to the Triassic granite; the early Yanshanian nonferrous metal mineralization period corresponding to the Jurassic granite, and the late Yanshanian gold and polymetallic mineralization period corresponding to the Cretaceous granite [65]. Further subdivision means that there were four periods of large-scale magmatic activity in the Mesozoic, namely Shidao granite in the Late Triassic, Linglong granite in the Late Jurassic, Guojialing granite in the early Cretaceous, Weideshan granite and Laoshan granite in the middle and late Early Cretaceous. Along with the large-scale magmatic activity, metal mineralization occurred. The mineralization of the Late Triassic, Late Jurassic and early Cretaceous are relatively weak. The middle and late Early Cretaceous is the "metallogenic explosion" stage [147], forming the widely distributed gold deposits in Jiaodong, accompanied by Cu, Pb, Zn and other nonferrous metal deposits.

The key markers of Jiaodong gold and polymetallic mineralization are magmatism, fluid activity and extensional structure. Extensive magmatic uplift and extensional structures in the Early Cretaceous in Jiaodong formed the extensional tectonic system [85]. During the formation of this system, a large proportion of crust and mantle materials were exchanged and mixed, and the fluid interaction was highly active [38], resulting in a magmatic fluid metallogenic system, which provided favorable metallogenic conditions for gold and nonferrous metal hydrothermal deposits. Thus, a large-scale explosive mineralization occurred in Jiaodong in the middle and late Early Cretaceous.

7. Conclusions

The intrusive age ranges of Linglong, Guojialing, Weideshan, and Laoshan granites are 155–154 Ma, 131–130 Ma, 118–111 Ma, and 116 Ma, respectively, which are basically in line with the previous age test data. Together with the Shidao granite (227–200 Ma), five phases of magmatism can be classified according to the time and geochemical features, all of which have different degrees of gold and polymetallic mineralization.

The type of granites evolved from A- and S-type to I- and A-type from the Late Triassic to the Early Cretaceous, and thus reflects the evolution of geodynamics in the Mesozoic, indicating the switch from NCC−YC collision to subduction of the PPP, with crustal thickening switching to lithospheric thinning, and a compressional tectonic setting changing to an extensional setting. The superposition and transformation of the tectonic system is closely related to the formation and temporal–spatial distribution of gold and polymetallic mineralization.

The key markers of Jiaodong gold and polymetallic mineralization are magmatism, fluid activity and extensional structure. Extensive magmatic uplift and extensional structures in the Early Cretaceous in Jiaodong formed the extensional tectonic system. During the formation process, a large proportion of crust and mantle materials exchanged and mixed, and the fluid interaction was highly active, resulting in a magmatic fluid metallogenic system, which provided favorable metallogenic conditions for gold and nonferrous metal hydrothermal deposits. Thus, a large-scale explosive mineralization occurred in Jiaodong in the middle and late Early Cretaceous.

Supplementary Materials: The following supporting information can be downloaded at: https://www.mdpi.com/article/10.3390/min12091073/s1, Table S1: Trace element compositions of the Mesozoic granite in the Jiaodong Peninsula [70,73,74,86,106,112,133], Table S2: Major element compositions of the Mesozoic granite in the Jiaodong Peninsula [70,73,74,86,133].

Author Contributions: Conceptualization, B.W., Z.D. and J.Z.; field investigation, B.W., Z.B. and J.L.; experimental analysis, C.L.; software, B.W. and Q.Z.; validation, Z.B. and S.W.; writing—original draft preparation, B.W.; writing—review and editing, B.W., Z.D. and M.S. All authors have read and agreed to the published version of the manuscript.

Funding: This work was supported by the National Natural Science Foundation of China-Shandong Joint Fund Project (No. U2006201), Youth Science and Technology Innovation Fund of Shandong Provincial No. 6 Exploration Institute of Geology and Mineral Resources (No. LY-QK-202203), High-level Scientific and technological Talents Innovation Team project of Shandong Provincial No. 6 Exploration Institute of Geology and Mineral Resources (LY-TD-202201), and Science and technology project of Shandong Provincial Bureau of Geology and Mineral Resources (No. KY202208).

Institutional Review Board Statement: Not applicable.

Informed Consent Statement: Not applicable.

Data Availability Statement: Data sharing is not applicable to this article.

Acknowledgments: The authors are grateful for the constructive comments by the anonymous reviewers.

Conflicts of Interest: The authors declare no conflict of interest.

References

1. Zhai, M.G.; Yang, J.H.; Liu, W.J. Large clusters of gold deposits and large–scale metallogenesis in the Jiaodong Peninsula, eastern China. *Sci. China Ser. D Earth Sci.* **2001**, *44*, 758–768. [CrossRef]
2. Ding, Z.J.; Sun, F.Y.; Liu, F.L.; Liu, J.H.; Peng, Q.M.; Ji, P.; Li, B.L.; Zhang, P.J. Mesozoic geodynamic evolution and metallogenic series of major metal deposits in Jiaodong Peninsula, China. *Acta Petrol. Sin.* **2015**, *31*, 3045–3080. (In Chinese with English abstract)
3. Song, M.C.; Song, Y.X.; Li, J.; Li, S.Y. Metallogenic Series of Gold and Nonferrous Metal Deposits Related to Cretaceous Granites in Eastern Shandong Peninsula, China. *Geotecton. Metallog.* **2015**, *39*, 823–843. (In Chinese with English abstract)
4. Chen, J.; Sun, F.Y.; Wang, L.; Wang, S.; Li, R.H. Zircon U–Pb geochronology and petrogeochemistry of Luanjiahe granite in Jiaodong region and their geological significance. *Glob. Geol.* **2015**, *34*, 283–295. (In Chinese with English abstract)
5. Geng, K.; Wang, R.J.; Li, H.K.; Liang, T.T.; Zhang, Y.B. Zircon SHRIMP U–Pb geochronology of Congjia granodiorite from northwest Jiaodong area. *Acta Geosci. Sin.* **2016**, *37*, 90–100. (In Chinese with English abstract)
6. Goss, C.S.; Wilde, S.A.; Wu, F.Y.; Yang, J.H. The age, isotopic signature and significance of the youngest Mesozoic granitoids in the Jiaodong Terrene, Shandong Province, North China Craton. *Lithos* **2010**, *120*, 309–326. [CrossRef]
7. Guan, K.; Luo, Z.K.; Miao, L.C.; Huang, J.Z. SHRIMP in zircon chronology for Guojialing suite granite in Jiaodong Zhaoye district. *Sci. Geol. Sin.* **1998**, *33*, 318–328, (In Chinese with English abstract).
8. Hu, S.L.; Wang, S.S.; Sang, H.Q.; Qiu, J.; Zhang, R.G. Isotopic ages of Linglong and Guojialing batholiths in Shandong Province and their geological implication. *Acta Petrol. Sin.* **1987**, *20*, 38–42. (In Chinese with English abstract)
9. Lin, B.L.; Li, B.L. Geochemistry, U–Pb dating, Lu–Hf isotopic analysis and geological significance of Linglong granite in Jiaodong Peninsula. *J. Chengdu Univ. Technol. Sci. Technol. Ed.* **2013**, *40*, 147–160. (In Chinese with English abstract)
10. Luo, X.D.; Yang, X.Y.; Duan, L.A.; Sun, W.D. Geochemical and geochronological study of the gold–related Guojialing pluton and Shangzhuang pluton in Jiaobei block. *Acta Geol. Sin.* **2014**, *88*, 1874–1888. (In Chinese with English abstract)
11. Miao, L.C.; Luo, Z.K.; Guan, K.; Huang, J.Z. The implication of the SHRIMP U–Pb age in zircon to the petrogenesis of the Linglong granite, east Shandong Province. *Acta Petrol. Sin.* **1998**, *14*, 198–206.
12. Qiu, L.G.; Ren, F.L.; Cao, Z.X.; Zhang, Y.Q. Late Mesozoic magmatic activities and their constraints on geotectonic of Jiaodong region. *Geotecton. Metallog.* **2008**, *32*, 117–123. (In Chinese with English abstract)
13. Sai, S.X.; Zhao, T.M.; Wang, Z.L.; Huang, S.Y.; Zhang, L. Petrogenesis of Linglong biotite granite: Constraints from mineralogical characteristics. *Acta Petrol. Sin.* **2016**, *32*, 2477–2493. (In Chinese with English abstract)
14. Sun, H.S.; Li, H.; Liu, L.; Chen, Q.M.; Yang, H.; Wu, P. Exhumation history of the Jiaodong and its adjacent areas since the Late Cretaceous: Constraints from low temperature thermo chronology. *Sci. China Earth Sci.* **2017**, *60*, 531–545. [CrossRef]
15. Wang, L.G.; Qiu, Y.M.; McNaughton, N.J. Constraints on crustal evolution and gold metallogeny in the northeastern Jiaodong Peninsula, China, from SHRIMP U–Pb zircon studies of granitoids. *Ore Geol. Rev.* **1998**, *13*, 275–291. [CrossRef]
16. Wang, Z.L.; Zhao, Y.X.; Zhan, Q.; Lu, H.W.; Li, J.L.; Cheng, W. Magma mixing for the high Ba–Sr Guojiling type granitoids in northwest Jiaodong Peninsula: Constraints from petrogeochemistry and Sr–Nd isotopes. *Acta Petrol. Sin.* **2014**, *30*, 2595–2608. (In Chinese with English abstract)
17. Yang, J.H.; Zhu, M.F.; Liu, W.; Zhai, M.G. Geochemistry and petrogenesis of Guojialing granodiorites from the northwestern Jiaodong Peninsula, eastern China. *Acta Petrol. Sin.* **2003**, *19*, 692–700. (In Chinese with English abstract)
18. Yang, K.F.; Fan, H.R.; Santosh, M. Reactivation of the Archean lower crust: Implications for zircon geochronology, elemental and Sr–Nd–Hf isotopic geochemistry of Late Mesozoic granitoids from northwestern Jiaodong Terrane, the North China Craton. *Lithos* **2012**, *146–147*, 112–127. [CrossRef]
19. Yang, Q.Y.; Santosh, M. Early Cretaceous magma flare–up and its implications on gold mineralization in the Jiaodong Peninsula, China. *Ore Geol. Rev.* **2015**, *65*, 626–642. [CrossRef]
20. Zhang, H.F.; Zhai, M.G.; He, Z.F.; Peng, P.; Xu, B.L. Petrogenesis and implications of the sodium–rich granites from the Kunyushan complex, eastern Shandong Province. *Acta Petrol. Sin.* **2004**, *20*, 369–380. (In Chinese with English abstract)

21. Zhang, H.F.; Zhai, M.G.; Tong, Y.; Peng, P.; Xu, B.L.; Guo, J.H. Petrogenesis of the Sanfoshan high Ba–Sr granite, Jiaodong Peninsula, eastern China. *Geol. Rev.* **2006**, *52*, 43–53. (In Chinese with English abstract)
22. Zhao, G.T.; Wang, D.Z.; Cao, Q.C. Thermal evolution and its significance of I–A type granitoid complex: The Laoshan granitoid as an example. *Sci. China Earth Sci.* **1998**, *41*, 529–536. [CrossRef]
23. Zhao, Z.F.; Zheng, Y.F. Remelting of subducted continental lithosphere: Petrogenesis of Mesozoic magmatic rocks in the Dabie–Sulu orogenic belt. *Sci. China Earth Sci.* **2009**, *52*, 1295–1318. [CrossRef]
24. Bi, S.J.; Zhao, X.F. $^{40}Ar/^{39}Ar$ dating of the Jiehe gold deposit in the Jiaodong Peninsula, eastern North China Craton: Implications for regional gold metallogeny. *Ore Geol. Rev.* **2017**, *86*, 639–651. [CrossRef]
25. Hu, F.F.; Fan, H.R.; Yang, J.H.; Wan, Y.S.; Liu, D.Y.; Zhai, M.G.; Jin, C.W. Mineralizing age of the Rushan lode gold deposit in the Jiaodong Peninsula: SHRIMP U–Pb dating on hydrothermal zircon. *Chin. Sci. Bull.* **2004**, *49*, 1629–1636. [CrossRef]
26. Li, H.M.; Mao, J.W.; Shen, Y.C.; Liu, T.B.; Zhang, L.C. Ar–Ar ages of K-feldspar and quartz from Dongji gold deposit, Northwest Jiaodong, and their significance. *Miner. Depos.* **2003**, *22*, 72–77. (In Chinese with English abstract)
27. Yang, J.H.; Zhou, X.H.; Chen, L.H. Dating of gold mineralization for super–large altered tectonite-type gold deposits in northwestern Jiaodong Peninsula and its implications for gold metellogeny. *Acta Petrol. Sin.* **2000**, *16*, 454–458. (In Chinese with English abstract)
28. Yang, J.H.; Zhou, X.H. The Rb–Sr isochron of ore and pyrite sub–samples from Linglong gold deposit, Jiaodong Peninsula, eastern China and their geological significance. *Chin. Sci. Bull.* **2000**, *45*, 2272–2276. [CrossRef]
29. Yang, J.H.; Zhou, X.H. Rb–Sr, Sm–Nd and Pb isotope systematics of pyrite: Implications for the age and genesis of lode gold deposits. *Geology* **2001**, *29*, 711–714. [CrossRef]
30. Zhang, L.C.; Shen, Y.C.; Liu, T.B.; Zeng, Q.D.; Li, G.M.; Li, H.M. $^{40}Ar/^{39}Ar$ and Rb–Sr isochron dating of the gold deposits on northern margin of the Jiaolai Basin, Shandong, China. *Sci. China Earth Sci.* **2003**, *46*, 708–718. [CrossRef]
31. Zhang, X.O.; Cawood, P.A.; Wilde, S.A. Geology and timing of mineralization at the Cangshang gold deposit, north–western Jiaodong Peninsula, China. *Miner. Depos.* **2003**, *38*, 141–153. [CrossRef]
32. Chen, B.; Deng, J.; Ji, X. Time Limit of Gold Mineralization in Muping–Rushan Belt, Eastern Jiaodong Peninsula, China: Evidence from Muscovite Ar–Ar Dating. *Minerals* **2022**, *12*, 278. [CrossRef]
33. Ding, Z.J. *Study on Metallogenic Regularity of Mesozoic Precious and Non-Ferrous Deposits in Jiaodong Peninsula*; Jilin University: Changchun, China, 2014; pp. 1–208. (In Chinese with English abstract)
34. Goldfarb, R.J.; Santosh, M. The dilemma of the Jiaodong gold deposits: Are they unique? *Geosci. Front.* **2014**, *5*, 139–153. [CrossRef]
35. Guan, K.; Luo, Z.K.; Miao, L.C.; Huang, J.Z. Petrochemical and geochemical charactristics of Guojialing suite in Zhaoyuan district and the genetic relation of gold mineralization to the granite. *Contrib. Geol. Miner. Resour. Res.* **1997**, *12*, 1–8. (In Chinese with English abstract)
36. Luo, Z.K.; Guan, K.; Miao, L.C. Discussion on relationship between lamprophyre veins and mineralization in the Linglong gold field, eastern Shandong. *Gold Geol.* **2001**, *7*, 15–21. (In Chinese with English abstract)
37. Xu, W.G.; Fan, H.R.; Yang, K.F.; Hu, F.F.; Cai, Y.C. Gold mineralizing efficiency during hydrothermal alteration of the Mesozoic granitoids in the northwest Jiaodong Peninsula: Contrasting conditions between the Guojialing and Linglong plutons. *Chem. Erde–Geochem.* **2017**, *77*, 387–398. [CrossRef]
38. Zhai, M.G.; Fan, H.R.; Yang, J.H.; Miao, L.C. Large–scale cluster of gold deposits in east Shandong: An orogenic metallogenesis. *Earth Sci. Front.* **2004**, *11*, 85–98. (In Chinese with English abstract)
39. Zhou, T.H.; Lu, G. Tectonics, granitoids and Mesozoic gold deposits in east Shandong, China. *Ore Geol. Rev.* **2000**, *16*, 71–90. [CrossRef]
40. Song, M.C.; Wang, P.C. *Regional Geology in Shandong Province*; Shandong Provincial Map Publishing House: Jinan, China, 2003; pp. 25–720. (In Chinese)
41. Tam, P.Y.; Zhao, G.C.; Sun, M.; Li, S.Z.; Iizuka, Y.; Ma, G.S.; Yin, C.Q.; He, Y.H.; Wu, M.L. Metamorphic P–T path and tectonic implications of medium–pressure pelitic granulites from the Jiaobei massif in the Jiao–Liao–Ji Belt, North China Craton. *Precambrian Res.* **2012**, *220*, 177–191. [CrossRef]
42. Tam, P.Y.; Zhao, G.C.; Zhou, X.W.; Sun, M.; Guo, J.H.; Li, S.Z.; Yin, C.Q.; Wu, M.L.; He, Y.H. Metamorphic P–T path and implications of high–pressure pelitic granulites from the Jiaobei massif in the Jiao–Liao–Ji Belt, North China Craton. *Gondwana Res.* **2012**, *22*, 104–117. [CrossRef]
43. Tang, J.; Zheng, Y.F.; Wu, Y.B.; Gong, B.; Liu, X.M. Geochronology and geochemistry of metamorphic rocks in the Jiaobei terrane: Constraints on its tectonic affinity in the Sulu orogen. *Precambrian Res.* **2007**, *152*, 48–82. [CrossRef]
44. Wan, Y.S.; Xie, H.W.; Yang, C.H.; Kröner, K.; Ma, M.Z.; Dong, C.Y.; Du, L.L.; Xie, H.Q.; Liu, D.Y. Early Neoarchean (~27 Ga) tectono–thermal events in the North China Craton: A synthesis. *Precambrian Res.* **2014**, *247*, 45–63. [CrossRef]
45. Zhou, J.B.; Wilde, S.A.; Zhao, G.C.; Zheng, C.Q.; Jin, W.; Zhang, X.Z.; Cheng, H. SHRIMP U–Pb zircon dating of the Neoproterozoic Penglai Group and Archean gneisses from the Jiaobei Terrane, North China Craton, and their tectonic implications. *Precambrian Res.* **2008**, *160*, 323–340. [CrossRef]
46. Tam, P.K.; Zhao, G.C.; Liu, F.; Zhou, X.; Sun, M.; Li, S.Z. Timing of metamorphism in the Paleoproterozoic Jiao–Liao–Ji Belt: New SHRIMP U–Pb zircon dating of granulites, gneisses and marbles of the Jiaobei massif in the North China Craton. *Gondwana Res.* **2011**, *19*, 150–162. [CrossRef]

47. Ding, Z.J.; Sun, F.Y.; Liu, D.H.; Zhang, P.J.; Yang, G.F.; Kong, Y. Metallogenic series of gold and polymetallic deposits in north Fushan area of Yantai city. *Shandong Land Resour.* **2011**, *27*, 1–6. (In Chinese with English abstract)
48. Sun, F.Y.; Ding, Z.J.; Liu, D.H.; Zhang, P.J.; Yu, X.F. Discussion on the porphyry metallogenic system in north Fushan area, Jiaodong peninsula. *Gold* **2011**, *32*, 14–19. (In Chinese with English abstract)
49. Li, S.Z.; Kusky, T.M.; Zhao, G.C.; Liu, X.C.; Zhang, G.W.; Kopp, H.; Wang, L. Two–stage Triassic exhumation of HP–UHP terranes in the western Dabie orogen of China: Constraints from structural geology. *Tectonophysics* **2010**, *490*, 267–293. [CrossRef]
50. Zhao, G.C.; Sun, M.; Wilde, S.A.; Li, S.Z. Late Archean to Paleoproterozoic evolution of the North China Craton: Key issues revisited. *Precambrian Res.* **2005**, *136*, 177–202. [CrossRef]
51. Zhao, H.G.; Sun, J.G.; Ling, H.F.; Shen, K.; Hou, S.X. Characteristics and geological significance of ore–forming fluids in the Jiaodong gold deposits. *Geol. Prospect.* **2005**, *41*, 27–33. (In Chinese with English abstract)
52. Hacker, B.R.; Ratschbacher, L.; Webb, L.; McWilliams, M.O.; Ireland, T.; Calvert, A.; Dong, S.; Wenk, H.R.; Chateigner, D. Exhumation of ultrahigh-pressure continental crust in east central China: Late Triassic-Early Jurassic tectonic unroofing. *J. Geophys. Res. Solid Earth* **2000**, *105*, 13339–13364. [CrossRef]
53. Ratschbacher, L.; Franz, L.; Enkelmann, E.; Jonckheere, R.; Porschke, A.; Hacker, B.R.; Dong, S.; Zhang, Y. The Sino–Korean–Yangtze suture, the Huwan detachment, and the Paleozoic–Tertiary exhumation of (ultra) high–pressure rocks along the Tongbai–Xinxian–Dabie Mountains. Ultrahigh–Pressure Metamorphic: Deep Continental Subduction. *Geol. Soc. Am.* **2006**, *403*, 45–77.
54. Ratschbacher, L.; Hacker, B.R.; Calvert, A.; Webb, L.E.; Grimmer, J.C.; McWilliams, M.O.; Ireland, T.; Dong, S.W.; Hu, J.M. Tectonics of the Qinling (Central China): Tectono stratigraphy, geochronology, and deformation history. *Tectonophysics* **2003**, *366*, 1–53. [CrossRef]
55. Xu, Z.; Zeng, L.; Liu, F.; Yang, J.; Zhang, Z.; McWilliams, M.; Liu, J.G. Polyphase subduction and exhumation of the Sulu High–pressure–ultrahigh–pressure metamorphic Terrane. *Geol. Soc. Am.* **2006**, *403*, 93–114.
56. Zheng, Y.F.; Fu, B.; Gong, B.; Li, L. Stable isotope geochemistry of ultrahigh pressure metamorphic rocks from the Dabie–Sulu orogen in China: Implications for geodynamics and fluid regime. *Earth Sci. Rev.* **2003**, *62*, 105–161. [CrossRef]
57. Zheng, Y.F.; Zhou, J.B.; Wu, Y.B.; Xie, Z. Low–grade metamorphic rocks in the Dabie–Sulu orogenic belt: A passive–margin accretionary wedge deformed during continent subduction. *Int. Geol. Rev.* **2005**, *47*, 851–871. [CrossRef]
58. Song, M.C.; Li, S.Z.; Santosh, M.; Zhao, S.J.; Yu, S.; Yi, P.H.; Cui, S.X.; Lv, G.X.; Xu, J.X.; Song, Y.X.; et al. Types, characteristics and metallogenesis of gold deposits in the Jiaodong Peninsula, Eastern North China Craton. *Ore Geol. Rev.* **2015**, *65*, 612–625. [CrossRef]
59. Wang, B.; Zhou, J.B.; Wilde, S.A.; Zhang, X.Z.; Ren, S.M. The timing of final closure along the Changchun–Yanji suture zone: Constraints from detrital zircon U–Pb dating of the Triassic Dajianggang Formation, NE China. *Lithos* **2016**, *261*, 216–231. [CrossRef]
60. Lv, G.X.; Kong, Q.C. *Geology of Linglong-Jiaojia Type Gold Deposit, Jiaodong*; Science Press: Beijing, China, 1993; pp. 1–266. (In Chinese)
61. Song, M.C.; Yi, P.H.; Cui, S.X.; Xu, J.X.; Zhou, M.L.; Jiang, H.L.; Huang, T.L.; Jiao, X.M.; Wan, G.P.; Cao, C.G. Thermal Uplifting Extension Ore forming Theory and Its Prospecting Significance in Jiaodong Gold Deposit. *Shandong Land Resour.* **2013**, *29*, 1–12. (In Chinese with English abstract)
62. Sun, F.Y.; Shi, Z.L.; Feng, B.Z. *Geology of Jiaodong Gold Deposit and C-H-O Fluid Differentiation and Mineralization of Mantle Source*; Jilin People's Publishing House: Changchun, China, 1995; pp. 1–170. (In Chinese)
63. Ding, Z.J.; Sun, F.Y.; Zhao, C.S.; Liu, D.H.; Zhang, P.J.; Wang, X.Q. Gold metallogenic series in northeast margin of Jiaolai Basin, Shandong Province. *Miner. Depos.* **2010**, *29*, 919–920. (In Chinese)
64. Song, M.C.; Zhang, J.J.; Zhang, P.J.; Yang, L.Q.; Liu, D.H.; Ding, Z.J.; Song, Y.X. Discovered and tectonic–magmatic background of super large gold deposit in offshore of northern Sanshandao, Shandong Peninsula, China. *Acta Geol. Sin.* **2015**, *89*, 365–383. (In Chinese with English abstract)
65. Ding, Z.J.; Sun, F.Y.; Liu, F.L.; Liu, J.H.; Liu, D.H.; Zhang, P.J.; Du, S.X.; Li, B. U–Pb dating of zircons from the Weideshan molybdenum copper polymetallic deposits in Jiaodong Peninsula, China, and its geological significance. *Acta Petrol. Sin.* **2013**, *29*, 607–618. (In Chinese with English abstract)
66. Zhou, J.B.; Zheng, Y.F.; Zhao, Z.F. Zircon U–Pb dating on Mesozoic granitoids at Wulian, Shandong Province. *Geol. J. China Univ.* **2003**, *9*, 185–194. (In Chinese with English abstract)
67. Zhu, C.Y.; Li, H.K.; Yu, X.F.; Geng, K.; Liang, T.T.; Zhang, Y.B. Structural Assemblage Classfication of Mesozoic Intrusive Rocks Associated with Gold Mineralization in Jiaodong Area. *Shandong Land Resour.* **2014**, *30*, 1–8. (In Chinese with English abstract)
68. Song, M.C.; Xun, J.X.; Wang, P.C. *Tectonic Framework and Tectonic Evolution of Shandong Province*; Geological Publishing House: Beijing, China, 2009; pp. 1–274. (In Chinese)
69. Wang, B.; Song, M.C.; Zhou, J.B.; Ding, Z.J.; Bao, Z.Y.; Lv, J.Y.; Wang, S.S. Four Stages A-type granitoids in Shandong Province and Their Implications for Tectonic Evolution. *N. China Geol.* **2022**, *in press*. (In Chinese with English abstract)
70. Chen, J.Z.; Jiang, N. Petrogenesis of the Late-Triassic alkaline magmatism in the Jiaodong area: Evidence from U-Pb age, Hf-O isotopes of zircons. *Acta Petrol. Sin.* **2011**, *27*, 3557–3574. (In Chinese with English abstract)
71. Chen, J.F.; Xie, Z.; Li, H.M.; Zhang, X.D.; Zhou, T.X.; Park, Y.S.; Ahn, K.S.; Chen, D.G.; Zhang, X. U–Pb zircon ages for a collision–related K–rich complex at Shidao in the Sulu ultrahigh pressure terrane, China. *Geochem. J.* **2003**, *37*, 35–46. [CrossRef]

72. Guo, J.H.; Chen, F.K.; Zhang, X.M.; Siebel, W.; Zhai, M.G. Evolution of syn- to post-collisional magmatism from north Sulu UHP belt, eastern China: Zircon U-Pb geochronology. *Acta Petrol. Sin.* **2005**, *21*, 1281–1301. (In Chinese with English abstract)
73. Xu, H.J.; Zhang, J.F.; Wang, Y.F.; Liu, W.L. Late Triassic alkaline complex in the Sulu UHP terrane: Implications for post–collisional magmatism and subsequent fractional crystallization. *Gondwana Res.* **2016**, *35*, 390–410. [CrossRef]
74. Yang, J.H.; Chung, S.L.; Wilde, S.A.; Wu, F.Y.; Chu, M.F.; Lo, C.H.; Fan, H.R. Petrogenesis of postorogenic syenites in the Sulu Orogenic Belt, East China: Geochronological, geochemical and Nd–Sr isotopic evidence. *Chem. Geol.* **2005**, *214*, 99–125. [CrossRef]
75. Deng, J.; Yang, L.Q.; Liu, W.; Sun, Z.S.; Li, X.Y.; Wang, Q.F. Gold origin and fluid ore-forming effect of Zhao-Ye ore deposits concentrating area in Jiaodong, Shandong, China. *Chin. J. Geol.* **2001**, *36*, 257–268. (In Chinese with English abstract)
76. Li, S.X.; Liu, C.C.; An, Y.H. *Geology of Jiaodong Gold Deposit*; Geological Publishing House: Beijing, China, 2007; pp. 1–471. (In Chinese)
77. Liu, Z.J.; Wang, J.P.; Zheng, D.W.; Liu, J.J.; Liu, J.; Fu, C. Exploration prospect and post-ore denudation in the northwestern Jiaodong Gold Province, China: Evidence from apatite fission track thermochronology. *Acta Petrol. Sin.* **2010**, *26*, 3597–3611. (In Chinese with English abstract)
78. Li, J. *Metallogenesis and Metallogenic Model of Mo-Cu-Pb-Zn Polymetallic Deposits in Jiaodong Area*; Chengdu University of Technology: Chengdu, China, 2012; pp. 1–127. (In Chinese)
79. Ding, Z.J.; Sun, F.Y.; Liu, J.H.; Liu, D.H.; Li, B.L.; Zhang, P.J.; Qian, Y.; Li, J. Re-Os dating of molybdenites from the Xingjiashan molybdenum-tungsten deposit in Jiaodong Peninsula, China and its geological significance. *Acta Petrol. Sin.* **2012**, *28*, 2721–2732. (In Chinese with English abstract)
80. Wiedenbeck, M.; Allé, P.; Corfu, F.; Griffin, W.L.; Meier, M.; Oberli, F.; Vonquadt, A.; Roddick, J.C.; Spiegel, W. Three natural zircon standards for U-Th-Pb, Lu-Hf, trace element and REE analyses. *Geostand. Newsl.* **1995**, *19*, 1–23. [CrossRef]
81. Reed, W.P. *Certificate of Analysis: Standard Reference Materials 610 and 611*; National Institute of Standards and Technology: Gaithersburg, MD, USA, 1992.
82. Hinton, R.W.; Upton, B.G.J. The chemistry of zircon: Variations within and between large crystals from syenite and alkali basalt xenoliths. *Geochim. Cosmochim. Acta* **1991**, *55*, 3287–3302. [CrossRef]
83. Hoskin, P.W.O.; Black, L.P. Metamorphic zircon formation by solid-state recrystallization of protolith igneous zircon. *J. Metamorph. Geol.* **2000**, *18*, 423–439. [CrossRef]
84. Rubatto, D. Zircon trace element geochemistry: Partitioning with garnet and the link between U–Pb ages and metamorphism. *Chem. Geol.* **2002**, *184*, 123–138. [CrossRef]
85. Song, M.C.; Li, J.; Li, S.Y.; Ding, Z.J.; Tan, X.F.; Zhang, Z.L.; Wang, S.J. Late Mesozoic thermal upwelling-extension structure in east Shandong Province and its geodynamic setting. *J. Jilin Univ. Earth Sci. Ed.* **2018**, *48*, 941–964. (In Chinese with English abstract)
86. Wang, B.; Song, M.C.; Huo, G.; Xu, Z.H.; Jiang, L.; Song, Y.X.; Li, J. Source characteristics and tectonic evolution of Late Mesozoic granites in Jiaodong and their implications for gold mineralization. *Acta Petrol. Mineral.* **2021**, *40*, 288–320. (In Chinese with English abstract)
87. Zhang, L.; Roberto, F.W.; Yang, L.Q.; Groves, D.I.; Deng, J. Mesozoic Orogenic Gold Mineralization in the Jiaodong Peninsula, China: A Focused Event at 120 ± 2 Ma During Cooling of Pregold Granite Intrusions. *Econ. Geol.* **2020**, *115*, 415–441. [CrossRef]
88. Li, S.G.; Xiao, Y.L.; Liou, D.L.; Chen, Y.Z.; Ge, N.J.; Zhang, Z.Q.; Sun, S.S.; Cong, B.L.; Zhang, R.Y.; Hart, S.R.; et al. Collision of the North China and Yangtze blocks and formation of coesite–bearing eclogites: Timing and processes. *Chem. Geol.* **1993**, *109*, 89–111. [CrossRef]
89. Li, S.G.; Wang, S.S.; Chen, Y.Z.; Liu, D.L.; Qiu, J.; Zhou, H.X.; Zhang, Z.M. Excess argon in phengite from eclogite: Evidence from dating of eclogite minerals by Sm–Nd, Rb–Sr and ^{39}Ar–^{40}Ar methods. *Chem. Geol.* **1994**, *112*, 343–350. [CrossRef]
90. Ames, L.; Zhou, G.; Xiong, B. Geochronology and geochemistry of ultrahigh–pressure metamorphism with implications for collision of the Sino–Korean and Yangtze cratons, central China. *Tectonics* **1996**, *15*, 422–489. [CrossRef]
91. Yang, J.S.; Xu, Z.Q.; Wu, C.L.; Liu, F.L.; Shi, R.D.; Wooden, J.; Maruyama, S. SHRIMP U-Pb Dating on Coesite Bearing Zircon: Evidence for Indosinian Ultrahigh-Pressure Metamorphism in Su-Lu, East China. *Acta Geol. Sin.* **2002**, *76*, 354–372. (In Chinese with English abstract)
92. Liu, F.L.; Xu, Z.Q.; Yang, J.S.; Zhang, Z.M.; Xue, H.M.; Li, T.F. Institute of Geology, Continental Dynamic Laboratory, Chinese Academy of Geological Sciences, Beijing 100037, China. Geochemical characteristics and UHP metamorphism of granitic gneisses in the main drilling hole of Chinese Continental Scientific Drilling Project and its adjacent area. *Acta Petrol. Sin.* **2004**, *20*, 9–26. (In Chinese with English abstract)
93. Liu, F.L.; Xu, Z.Q.; Song, B. Determination of UHP and Retrograde Metamorphic Ages of the Sulu Terrane: Evidence from SHRIMP U-Pb Dating on Zircons of Gneissic Rocks. *Acta Geol. Sin.* **2003**, *77*, 229–237. (In Chinese with English abstract)
94. Gao, T.S.; Chen, J.F.; Xie, Z.; Yan, J.; Qian, H. Geochemistry of Triassic igneous complex at Shidao in the Sulu UHP metamorphic belt. *Acta Petrol. Sin.* **2004**, *20*, 1025–1038. (In Chinese with English abstract)
95. Song, M.C.; Song, Y.X.; Ding, Z.J.; Wei, X.F.; Sun, S.L.; Song, G.Z.; Zhang, J.J.; Zhang, P.J.; Wang, Y.G. The discovery of The Jiaojia and the Sanshandao giant gold deposits in Jiaodong Peninsula and discussion on the relevant issues. *Geotecton. Metallog.* **2019**, *43*, 92–110. (In Chinese with English abstract)
96. Xu, H.L.; Zhang, D.Q.; Sun, G.Y. Characteristics and genesis of Kunyushan granite and its relation with gold deposits in Jiaodong. *Acta Petrol. Mineral.* **1997**, *16*, 131–143. (In Chinese with English abstract)

97. Li, J.J.; Luo, Z.K.; Liu, X.Y.; Xu, W.D.; Luo, H. Geodynamic setting for formation of large-superlarge gold deposits and Mesozoic granites in Jiaodong area. *Miner. Depos.* **2005**, *24*, 361–372. (In Chinese with English abstract)
98. Tan, J.; Wei, J.H.; Guo, L.L.; Zhang, K.Q.; Yao, C.L.; Chen, J.P.; Li, H.M. Zircon LA-ICP-MS U-Pb dating and phenocryst EPMA study of dikes in Guocheng area, Jiaodong: Implications for lithospheric evolution. *Sci. China Ser. D* **2008**, *38*, 913–929. (In Chinese with English abstract)
99. Zhang, T.; Zhang, Y.Q. Late Mesozoic tectono-magmatic evolution history of the Jiaobei uplift, Shandong Peninsula. *Acta Geol. Sin.* **2008**, *82*, 1210–1228. (In Chinese with English abstract)
100. Zhang, J.; Zhao, Z.F.; Zheng, Y.F.; Dai, M. Postcollisional magmatism: Geochemical constraints on the petrogenesis of Mesozoic granitoids in the Sulu orogen, China. *Lithos* **2010**, *119*, 512–536. [CrossRef]
101. Wang, S.J.; Wan, Y.S.; Wang, W.; Song, Z.Y.; Wang, J.G.; Dong, C.Y.; Xie, H.Q.; Liu, Q.D. Forming ages of granites in Laoshan area of Shandong Province—zircon SHRIMP U-Pb dating. *Shandong Land Resour.* **2010**, *26*, 1–6. (In Chinese with English abstract)
102. Wang, S.J.; Wan, Y.S.; Guo, R.P.; Song, Z.Y.; Wang, L.F. SHRIMP zircon dating of Linglong type (super unit) granite in eastern Shandong Province. *Shandong Land Resour.* **2011**, *27*, 1–7. (In Chinese with English abstract)
103. Ma, L.; Jiang, S.Y.; Dai, B.Z.; Jiang, Y.H.; Hou, M.L.; Pu, W.; Xu, B. Multiple sources for the origin of Late Jurassic Linglong adakitic granite in the Shandong Peninsula, Eastern China: Zircon U-Pb geochronological, geochemical and Sr-Nd-Hf isotopic evidence. *Lithos* **2013**, *162*, 251–263. [CrossRef]
104. Ma, L.; Jiang, S.Y.; Hou, M.L.; Dai, B.Z.; Jiang, Y.H.; Yang, T.; Zhao, K.D.; Pu, W.; Zhu, Z.Y.; Xu, B. Geochemistry of Early Cretaceous calc–alkaline lamprophyres in the Jiaodong Peninsula: Implication for lithospheric evolution of the eastern North China Craton. *Gondwana Res.* **2014**, *25*, 859–872. [CrossRef]
105. Dong, X.; Li, D.P.; Zhao, R.; Wang, X.R.; Wang, Q.F. Zircon U-Pb chronology and petrogenesis of Zetou pluton in the Jiaodong Peninsula: Implications for regional petrogenesis and mineralization in the Aptian to Albian. *Acta Petrol. Sin.* **2020**, *36*, 1501–1514, (In Chinese with English abstract).
106. Song, Y.X.; Yu, X.F.; Li, D.P.; Geng, K.; Yu, P.F.; Zuo, X.M.; Wang, X.F. Petrogenesis of the Beijie pluton from the northwestern Jiaodong Peninsula: Constraints from zircon U-Pb age, petrogeochemistry and Sr-Nd-Pb isotopes. *Acta Petrol. Sin.* **2020**, *36*, 1477–1500. (In Chinese with English abstract)
107. Song, M.C.; Song, Y.X.; Ding, Z.J.; Li, S.Y. Jiaodong gold deposits: Essential characteristics and major controversy. *Gold Sci. Technol.* **2018**, *26*, 406–422. (In Chinese with English abstract)
108. Huang, T.; Yang, L.Q.; Liu, X.D.; Li, H.L.; Zhang, B.L.; Wang, J.G.; Zhao, Y.F.; Zhang, N. Crustal evolution of the Jiaobei terrane Evidence from U-Pb ages, trace element compositions and Hf isotopes of inherited zircons of the Linglong biotite granite. *Acta Petrol. Sin.* **2014**, *30*, 2574–2594.
109. Wu, M.L.; Zhao, G.C.; Sun, M.; Li, S.Z. A synthesis of geochemistry and Sm–Nd isotopes of Archean granitoid gneisses in the Jiaodong Terrane: Constraints on petrogenesis and tectonic evolution of the Eastern Block, North China Craton. *Precambrian Res.* **2014**, *255*, 885–899. [CrossRef]
110. Song, M.C.; Wang, S.S.; Yang, L.X.; Li, J.; Li, S.Y.; Ding, Z.J. Metallogenic Epoch and Geological Significance of Nonferrous Metallic and Silver Deposits in Jiaodong Peninsula, China. *Acta Geol. Sin. Engl. Ed.* **2017**, *91*, 1305–1325. [CrossRef]
111. Yang, J.H.; Wu, F.Y.; Wilde, S.A. A review of the geodynamic setting of large–scale Late Mesozoic gold mineralization in the North China Craton: An association with lithospheric thinning. *Ore Geol. Rev.* **2003**, *23*, 125–152. [CrossRef]
112. Song, M.C.; Zhou, J.B.; Song, Y.X.; Wang, B.; Li, S.Y.; Li, J.; Wang, S.S. Mesozoic Weideshan granitoid suite and its relationship to large-scale gold mineralization in the Jiaodong Peninsula, China. *Geol. J.* **2020**, *55*, 5703–5724. [CrossRef]
113. Hu, F.F.; Fan, H.R.; Yang, J.H.; Zhai, M.G.; Jin, C.W.; Xie, L.W.; Yang, Y.H. Magma mixing for the origin of granodiorite: Geochemical, Sr–Nd isotopic and zircon Hf isotopic evidence of dioritic enclaves and host rocks from Changshannan granodiorite in the Jiaodong Peninsula, eastern China. *Acta Petrol. Sin.* **2005**, *21*, 569–586. (In Chinese with English abstract)
114. Yan, Q.S.; Metcalfe, I.; Shi, X.F.; Zhang, P.Y.; Li, F.C. Early Cretaceous granitic rocks from the southern Jiaodong Peninsula, eastern China: Implications for lithospheric extension. *Int. Geol. Rev.* **2018**, *61*, 821–838. [CrossRef]
115. Liu, J.M.; Zhang, H.F.; Sun, J.G.; Ye, J. Geochemical research on C–O and Sr–Nd isotopes of mantle–derived rocks from Shandong Province, China. *Sci. China Earth Sci.* **2004**, *47*, 171–180. [CrossRef]
116. Yan, J.; Chen, J.F.; Xie, Z.; Gao, T.S.; Foland, K.A.; Zhang, X.D.; Liu, M.W. Later Cretaceous basalts and mantle-derived xenoliths from eastern Shandong. *Acta Petrol. Sin.* **2005**, *21*, 99–112. (In Chinese with English abstract)
117. Eby, G.N. The A–type granitoids: A review of their occurrence and chemical characteristics and speculation on their petrogenesis. *Lithos* **1990**, *26*, 115–134. [CrossRef]
118. Picher, W.S. *Granite Type and Tectonic Environment. Mountain Building Processes*; Academic Pressa: London, UK, 1983; pp. 19–40.
119. Bedard, J. Enclaves from the A–type granite of the Meganic Complex, White Mountain magma series: Clues to granite magma genesis. *J. Geophys.* **1990**, *95*, 17797–17819. [CrossRef]
120. Chen, H.F.; He, S.Y.; Zhang, A.K.; Sun, J.L.; Yan, Z.P.; Liu, J.L.; Zhang, L.; Qian, Y. Petrogenesis and tectonic setting of Middle Silurian A-type granite in Kaerqueka area, East Kunlun. *Geol. Bull. China* **2021**, *40*, 1380–1393. (In Chinese with English abstract)
121. Whalen, J.B.; Jenner, G.A.; Longstaffe, F.J.; Robert, F.; Garipy, C. Geochemical and Isotopic (O, Nd, Pb and Sr) Constraints on A–type Granite Petrogenesis Based on the Topsails Igneous Suite, New foundland Appalachians. *J. Petrol.* **1996**, *37*, 1463–1489. [CrossRef]

122. Jia, X.H.; Wang, Q.; Tang, G.J. A type Granites: Research Progress and Implications. *Geotecton. Metallog.* **2009**, *33*, 465. (In Chinese with English abstract)
123. Zhang, Q.; Ran, H.; Li, C.D. A-type granite: What is the essence? *Acta Petrol. Sin.* **2012**, *31*, 621–626. (In Chinese with English abstract)
124. Loiselle, M.C.; Wones, D.R. *Characteristics and Origin of Anorogenic Granites*; Geological Society of America (Abstracts with Programs): Boulder, CO, USA, 1979; Volume 11, pp. 448–468.
125. Wu, S.P.; Wang, M.Y.; Qi, K.J. Present situation of researches on A-type granites: A review. *Acta Petrol. Sin.* **2007**, *26*, 57–66. (In Chinese with English abstract)
126. Sylvester, P.J. Post–collisional alkaline granites. *J. Geol.* **1989**, *97*, 261–280. [CrossRef]
127. Turner, S.; Sandiford, M.; Feden, J. Some geodynamic and compositiona1 constraints on "postorogenic" magmatism. *Geology* **1992**, *20*, 931. [CrossRef]
128. Wang, D.Z.; Zhao, G.T.; Qiu, J.S. The Tectonic Constraint on the Late Mesozoic A-type Granitoid in eastern China. *Geol. J. Univ.* **1995**, *1*, 13–21. (In Chinese with English abstract)
129. Sun, D.Y.; Wu, F.Y.; Li, H.M.; Lin, Q. Age of A-type granite after orogenic belt in northwestern Xiaoxinganling and its relationship with the eastern extension of Suolunshan-Hegenshan-Zdalaite collision zone. *Chin. Sci. Bull.* **2000**, *45*, 2217–2222. (In Chinese with English abstract)
130. Zhao, J.; Zhang, C.L.; Guo, X.J.; Liu, X.Y.; Wang, Q. Determination of the 2.4Ga A-type granite in Lvliang area of the North China Craton and its geological significance. *Acta Petrol. Sin.* **2015**, *31*, 1606–1620. (In Chinese with English abstract)
131. Sun, D.Y.; Wu, F.Y.; Gao, S.; Lu, X.P. Confirmation of two episodes of A-type granite emplacement during Late Triassic and Early Jurassic in the central Jilin Province, and their constraints on the structural pattern of Eastern Jilin Heilongjiang Area, China. *Earth Sci. Front.* **2005**, *12*, 263–275. (In Chinese with English abstract)
132. King, P.L.; White, A.J.R.; Chappell, B.W.; Allen, C.M. Characterization and Origin of Aluminous A–type Granites from the Lachlan Fold Belt, Southeastern Australia. *J. Petrol.* **1997**, *38*, 371–391. [CrossRef]
133. Zhao, G.T.; Wang, D.Z.; Cao, Q.C. The geochemistry and genesis of the Laoshan granitoids, Shandong Province. *Geol. J. China Univ.* **1997**, *3*, 1–15. (In Chinese with English abstract)
134. Chu, H.; Zhang, J.R.; Wei, C.J.; Wang, H.C.; Kang, J.L. Multiple phases of metamorphism during Paleozoic-Mesozoic and the implication for the tectonic evolution of northern North China: Research progresses and Prospects of "The Paleozoic metamorphism and tectonic dynamics in North China". *Geol. Surv. Res.* **2020**, *43*, 186–197. (In Chinese with English abstract)
135. Collins, W.J.; Beams, S.D.; White, A.J.R.; Chappell, B.W. Nature and origin of A–type granites with particular reference to southeastern Australia. *Contrib. Mineral. Petrol.* **1982**, *80*, 189–200. [CrossRef]
136. Pearce, J.A.; Harris, N.B.W.; Tindle, A.G. Trace element discrimination diagrams for the tectonic interpretation of granitic rocks. *J. Petrol.* **1984**, *25*, 956–983. [CrossRef]
137. Batchelor, R.A.; Bowden, P. Petrogenetic Interpretation of Granitoid Rock Series Using Multicationic Parameters. *Chem. Geol.* **1985**, *48*, 43–55. [CrossRef]
138. Ma, L.; Jiang, S.Y.; Hofmann, A.W.; Dai, B.Z. Lithospheric and asthenospheric sources of lamprophyres in the Jiaodong Peninsula: A consequence of rapid lithospheric thinning beneath the North China Craton? *Geochim. Cosmochim. Acta* **2014**, *124*, 250–271. [CrossRef]
139. Song, M.C. Jiaodong type gold deposit and its metallogenic tectonic magmatic background. *Miner. Depos.* **2014**, *33*, 131–132. (In Chinese with English abstract)
140. Wang, L.M.; Song, M.C.; Wang, P.C.; Wang, S.J.; Song, Z.Y.; Liu, J.W.; Li, Y.Y.; Zhang, X.D. *Structure and Evolution of Sulu ULTRAHIGH–Pressure (UHP) Metamorphic Belt*; Geological Publishing House: Beijing, China, 2005; pp. 1–126. (In Chinese)
141. Han, Y.W.; Ma, Z.D. *Geochemistry*; Geological Publishing House: Beijing, China, 2003; pp. 1–370.
142. Isozaki, Y. Jurassic accretion tectonics of Japan. *Island Arc* **1997**, *6*, 25–51. [CrossRef]
143. Maruyama, S.; Isozaki, Y.; Kimura, G.; Terabayashi, M. Paleogeographic maps of the Japanese islands: Plate tectonic systhesis from 750Ma to the resent. *Island Arc* **1997**, *6*, 121–142. [CrossRef]
144. Zhang, H.F.; Zhou, M.; Sun, M.; Zhou, X.H. The origin of Mengyin and Fuxian diamond iferous kimberlites from the north China Craton: Implication for Paleozoic subducted oceanic slab–mantle interaction. *J. Asian Earth Sci.* **2010**, *37*, 425–437. [CrossRef]
145. Ma, M.; Zhang, C.; Li, Y.; Gao, M.; Gao, J.; Li, S.; Feng, Q.; Li, J.; Tao, C.; Liu, Y. Geochronological, Geochemical and Sr-Nd-Pb-Hf Isotopic Constraints on the Petrogenesis of Pyroxene Diorites in the Sanchahe Iron-Gold Deposit, Western Shandong. *Minerals* **2022**, *12*, 601. [CrossRef]
146. Song, M.C.; Yang, L.Q.; Fan, H.R.; Yu, X.F.; Ding, Z.J.; Zhang, Y.W.; Qiu, K.F.; Li, J.; Zhang, L.; Wang, B.; et al. Current progress of metallogenic research and deep prospecting of gold deposits in the Jiaodong Peniusula during 10 years for Exploration Breakthrough Strategic Action. *Geol. Bull. China* **2022**, *41*, 903–935.
147. Hua, Z.M.; Mao, J.W. A preliminary discussion on the Mesozoic metallogenic explosion in east China. *Miner. Depos.* **1999**, *18*, 300–308. (In Chinese with English abstract)